

## Author's response to referee comments on "Buoyant forces promote tidewater glacier iceberg calving through large basal stress concentrations"

**Authors:** Trevers, M., Payne, A. J., Cornford, S. L., Moon, T.

The Cryosphere Discuss., <https://doi.org/10.5194/tc-2018-212>

We would like to thank both reviewers for their constructive and insightful criticisms and comments on our manuscript. These are taken account of in our revised manuscript. Here we reply to the more important criticisms.

Below, we respond to all comments from both reviews. Reviewer comments, numbered chronologically, are in italics, and the author response in plain text. Details of all changes to the manuscript to address comments are highlighted in bold text. References to the location in the manuscript of changes refer to the revised manuscript *without* markup displayed

### Reviewer #1

1. *I'm sorry, but so much of the discussion in the manuscript depends on un-referenced and un-explained "references to previous work" that I think that the manuscript needs to be revised significantly. The specific places where the discussion and explanations are inadequate are listed below.*

We agree that the exposition of the proposed mechanism inducing the stress concentrations is not entirely clear, and that we've also used some jargon in some places that hasn't been properly defined for the reader. Rewording and some additional exposition will be added to the manuscript, with detail of the changes given in response to specific comments below.

**No changes made in response to this specific comment. Changes that account for this general comment are detailed in response to comment #11**

2. *Other than the expository problem with the manuscript. I find the science compelling and well done. The work is creative and important in the study of iceberg calving mechanisms. Here's the stuff that needs attention (in my estimation):*

Thank you very much for the generous remark, we're glad that you found the work compelling!

**No changes made in response to this comment.**

3. *I wonder if the title really does justice. . . the paper is about bending moments (viscous and plastic bodies have bending moments too!) generated by geometry changes at the ice front due to ice/ocean and ice/atmosphere and ice/wave interactions. . . the present title could be misunderstood to represent "same old basal shear stress" stuff. . .*

The paper is not specifically about bending moments but rather about forces generated at the bed instantaneously at the onset of bending in response to the perturbation. Some further explanation is required on this for clarity (see the response to the next comment), but as such, we do not intend to change the title.

**No changes made in response to this specific comment.**

4. *line 13 - would it be more accurate to say "viscous bending moment" (remember you can bend a beam viscously and elastically and viscoelastically) leading to high tensile stress concentration at the bed. . . instead of stresses at the ice-bed interface? Who cares what the stresses are at the interface if the ice is actually in a state of bending induced fracture?*

As above, we don't attribute these stresses to a bending moment. We attribute these longitudinal stresses as those required to balance the abrupt decrease in basal shear across the grounding zone.

**We have added a new paragraph starting at page 8, line 4 to clarify and justify our interpretation of these stresses.**

5. *line 29 - Would this be a place to add a reference to Weertman?*

**A reference to Weertman (1957) for the Weertman sliding law has been added to page 4, line 7. Lines 7-9 of page 4 have been slightly reworded to account for this addition.**

6. *line 18 page 2 - The rotation should be indicated as "bottom out".*

**The description has been changed to refer to "bottom-out" calving events in page 2 line 10, page 2 line 19 and the caption for figure 1.**

7. *line 8 page 3 - If I were to be pedantic, I would say that a reference should be given for "Stokes equations" (in actuality, Stokes was prolific and probably has many equations associated with his name). Ditto for "Glen's flow law". . . a reference should be given.*

**A reference to Gagliardini et al. (2013) which solves to same Stokes equations has been provided on page 3 line 9. A reference to Glen (1958) has been provided on page 3 line 13.**

8. *line 1 page 4 - Is Cauchy stress the same as deviatoric stress?*

The deviatoric stress indicates the deviation from the Cauchy (or full) stress, i.e. it negates the average pressure term. For our ~1km thick glacier, the pressure will be ~10MPa everywhere along the bed and therefore the Cauchy stress, ignoring additional water pressure, will be compressive everywhere.

**This detail has been clarified in the paper with an adjustment to equation 2, and changes to the text in page 3 lines 10-12. Also, removal of text in page 4, line 1 which was rendered redundant. The identity matrix was added to table 1.**

9. *line 9 page 5 - Just out of curiosity why are 191 and 644 meters so precisely known as to be significant to the single meter? Can the authors tell us what would happen if the numbers were 192 and 643?*

These numbers are part of the model output and the precision is fairly arbitrary. The precision of these numbers is not important to our argument, and is in a small part determined by the mesh resolution (i.e. the peak occurs at a mesh node). Since it is not possible to identify locations to the nearest meter in the figures provided, we will change to reporting them as "approximately 190 m" and similarly for other such numbers.

**Changes made to: page 5, line 23; page 5, line 25; page 6, line 2; figure captions for figures 4, 5, 8, 9, 10.**

10. *section 3.1 - What is the a priori reason to expect water pressure to be significantly important in the problem? is it for promoting fracture propagation or is it for lubricating the base?*

The significance is that the mechanism we suggest relies on the abrupt reduction in basal shear stress where the ice ungrounds to produce the longitudinal stresses to balance this. If we apply a sliding law where the basal shear stress reduces gradually as a function of effective pressure, we wouldn't expect the same result.

**A sentence has been added to page 7, line 4 to clarify the expectation of different results with a different sliding law.**

11. line 4 page 7 - What is “Weertman-like”???? This seems to come in out of the blue. . . Weertman published hundreds of papers in his life, what is referred to here?

line 1 page 9 - Notch-triggered rotation mechanism was shown to be irrelevant under the full School regime”. . . Readers will get confused here, because “full School regime” is a weak form of jargon that doesn’t really convey the precise ideas (regardless of whether they are published in Schoof. . . my hunch is that the authors have a different meaning, i.e., an interpretation that they ascribe to the term “full School regime”)

line 12 and 13 page 9 - “Weertman . . . regime”???? Weertman-like stress peak???? What is this, and why the name Weertman???? Seems like citations and explanations are required. The discussion is flawed because it relies on readers having prior knowledge of what a “Weertman regime” is...

I’ve grouped these comments together because they all refer to the same thing. We agree with the reviewer that we’ve used jargon, the meaning of which has been poorly conveyed to the reader. When referring to “regimes”, we meant the use of the Weertman or Schoof sliding law. The “full” Schoof regime referred to the use of the Schoof sliding law with full hydrostatic water pressure applied along the ice-bed interface. “Weertman-like stress peak” referred to stress concentrations that have a similar profile to those produced using the Weertman sliding law.

**Numerous minor changes to the text have been made to clarify this: Page 7, line 27; page 10, line 7; page 10, lines 18-20.**

## Reviewer #2

1. *There is one major issue with the analysis, which is that the authors compare longitudinal deviatoric stress with a yield strength estimate from Vaughan (1993). The longitudinal deviatoric stress is problematic for two reasons. First, the various components of the deviatoric stress are not coordinate system invariant and have little physical meaning: a different coordinate system would result in different numbers. It is possible that the authors want to look at, say the components of the traction along the bed (which is well defined) or the largest principle deviatoric stress (which is also well defined). But this raises the more fundamental issue: it is the largest principle Cauchy stress and not the deviatoric stress that controls tensile fracture. And it is clear from the manuscript that the authors are fully focused on tensile basal crevasses. If the authors want to argue that the stresses are sufficient to trigger a tensile basal crevasse then they need to examine the largest principle Cauchy stress. Fortunately, this should be straightforward to compute from the full Stokes model. More problematically for the analysis performed here, for a kilometer thick glacier, the hydrostatic pressure is probably of the order of 10 MPa and may result in a negative (compressive) largest principle Cauchy stress. I should point that this is a common problem when dealing with failure of ice and especially basal crevasses. The most common solution to this problem is to (rather arbitrarily) superpose a hydrostatic pressure associated with water to the largest principle Cauchy stress to simulate the effect of water filled crevasses. This is commonly done and I think the authors could get away with it here if they want. Technically, you can’t really do this and the right way to do it is to calculate the Cauchy stress after introducing an infinitely narrow test crack. Doing it the right way, usually results in a compressive stress when using the power-law creep rheology of ice. If the authors go the usual route of superposing a hydrostatic stress field, I do suggest showing the stress with and without water pressure to emphasize that the water pressure is (or is not) critical.*

We have recalculated stresses using the recommended metric of the largest principle stress plus the water pressure, referred to as Effective Principle Stress (EPS) in Benn et al. (2017):

$$\text{EPS} = \sigma_1 + p_w = \frac{\sigma_{xx} + \sigma_{yy}}{2} + \sqrt{\left(\frac{\sigma_{xx} - \sigma_{yy}}{2}\right)^2 + \sigma_{xy}^2} + p_w$$

Unsurprisingly, the resultant stress profiles are similar to those reported in that paper. There is a large concentration of EPS in the location where the longitudinal deviatoric stress ( $\tau_{xx}$ ) peaks. The downstream compressive stress peak and the tensile peak located directly at the bottom corner of the calving front are comparatively greatly diminished in EPS as compared with the same features in  $\tau_{xx}$ . Figures AC1 and AC2 below compare  $\tau_{xx}$  and EPS calculated for the example reported in figure 4 of the original submission.

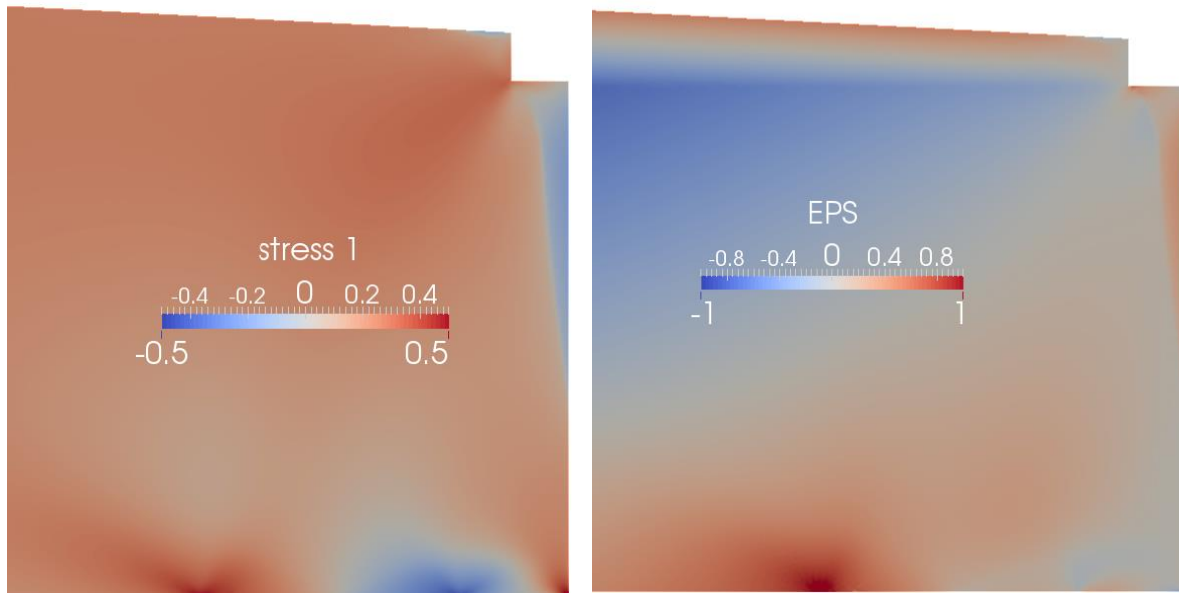


**Fig AC1.** Comparison of  $\tau_{xx}$  (left) and EPS calculated for the geometry shown in Figure 4. of the original submission. Units of stress in MPa. The spatial scale is the same as Figure 4. of the original submission.

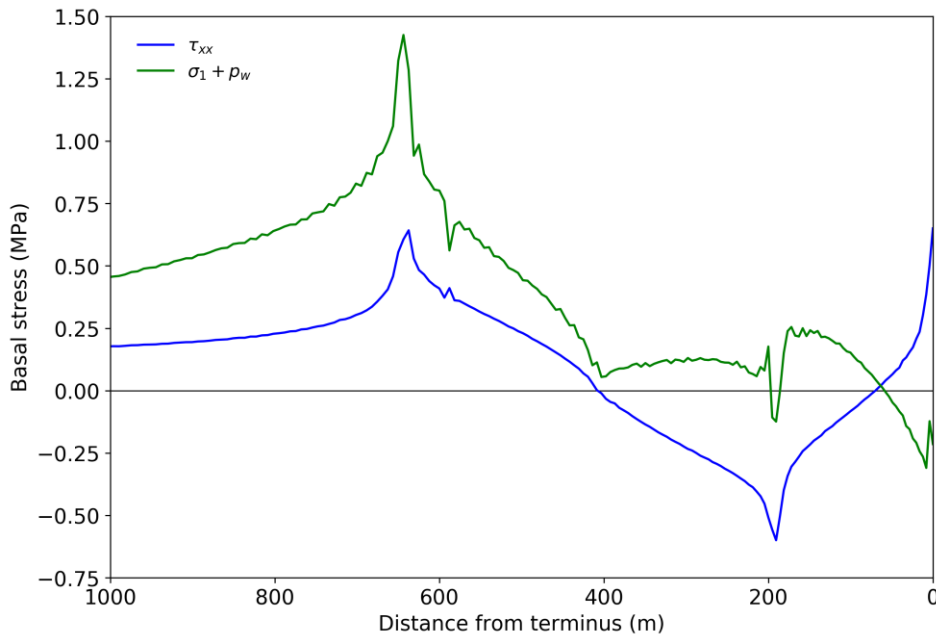


**Fig AC2.** Comparison of  $\tau_{xx}$  and EPS along the basal boundary, for the same geometry as in Figure AC1.

As the reviewer points out, the ice hydrostatic pressure is of order  $\sim 10\text{MPa}$  at the bed and therefore without the addition of the water pressure, the largest principle stress  $\sigma_1$  is negative everywhere. It was suggested that we add a plot to show that the water pressure is critical to produce a positive stress. We feel that this would be unnecessary and not particularly instructive, since  $p_w$  has a

constant value of 9.1MPa along the bed. However we will add a sentence to make it clear that the addition of  $p_w$  is critical to our analysis.

The reviewer suggests that the more correct way to carry out the analysis would be to introduce test cracks into the geometry and look at the crack tip stress. We have looked at this (Fig. AC3), but this problem has the stress tend to infinity approaching the crack tip, so that although our simulations do indicate a substantial stress around the tip, the numerical solutions do not converge with mesh resolution.

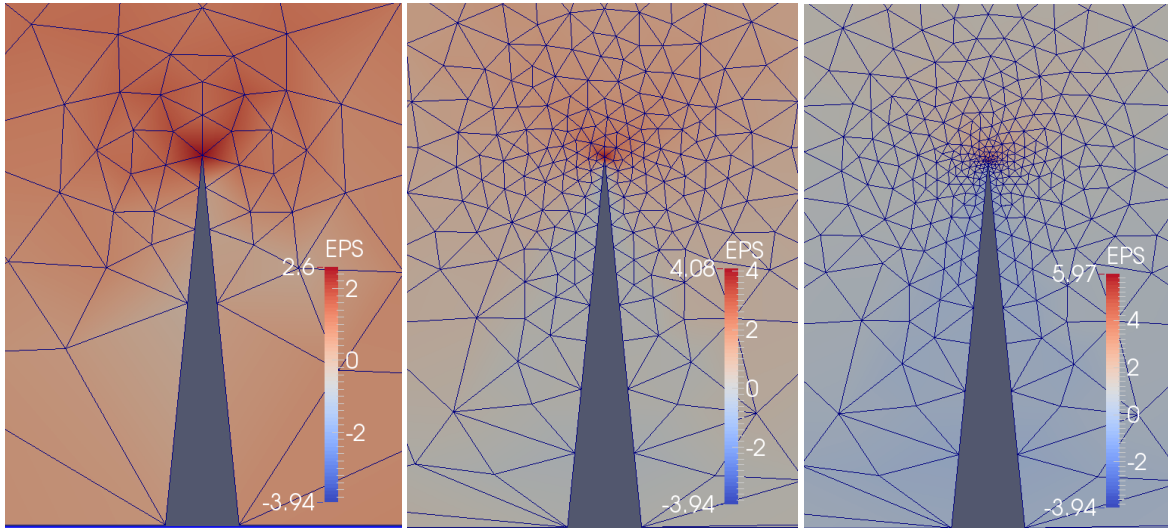


**Fig AC3.** Demonstration of the dependence of the crack tip stress upon the mesh spacing, with increasing resolution from left to right. The crack is 1m wide at the base, 5m high and located at the position of maximum basal EPS. In each figure, the maximum EPS on the colour bar corresponds to the value of EPS at the crack tip.

One approach to avoid this issue and test the likelihood of the crack to grow or stagnate would be to use the methods of linear elastic fracture mechanics (LEFM) to calculate a stress intensity factor for the crack tip (e.g. van der Veen, 1998; Krug et al., 2014).

We feel that following this method would entail a significant extra addition to the paper at this stage. Therefore our preferred choice is to use the EPS metric. Using this metric, the substantial growth in concentrated EPS following the geometric perturbation would lead to the formation of a crevasse at the same location as the original deviatoric stress metric. Other similar modelling studies (e.g. Nick et al., 2010; Todd et al., 2014) apply the Nye zero stress criterion (Nye, 1957) to calculate the depth of crevasses. Although we do not calculate crevasse depths, we will refer to this criterion so relate the high stresses to locations where crevasses will form.

**The following changes were made to account for this:**

- **Addition of section 2.3**
- **Figure 3 and caption**
- **Figure 4 and caption**
- **Figure 5 and caption**
- **Figure 7 and caption**
- **Figure 8 replotted as two figures, figure 8 and figure 9. This is to account for the large shift in the vertical scale when switching to the EPS metric.**
- **Figure 9 replotted and caption updated (and changed to figure 10)**
- **Changed “longitudinal deviatoric stress” to “EPS” at page 5, line 20.**
- **Removal of the reference to a tensile strength from Vaughan (1993) at page 5, line 21.**
- **Removal of the reference to tensile strength at page 5, line 25.**
- **Added sentence at page 5, line 28.**

- Updated text at page 7, lines 12 – 15 to account for changed figures and the updated results.
- Changed text at page 10, line 12 to account for the updated results using EPS.
- EPS and  $\sigma_1$  added to table 1.

2. *Another aspect of the analysis that is somewhat problematic is that the authors are comparing their stress metric to the yield strength estimated by Vaughan (1993). My understanding, however, is that Vaughan (1993) examined various yield strength envelopes, finding that the Von Mises stress envelope provided the best fit to the observations. The Von Mises yield criterion, however, is only equivalent to tensile failure in uniaxial loading, which is not the case for the model considered here. Recalling that the second deviatoric stress invariant is proportional to the Von Mises stress, what I suggest is that in addition to the largest principle Cauchy stress, the authors also consider showing the second deviatoric stress invariant as an additional stress metric. This stress metric can be more directly compared with Vaughan's estimated yield strength. Note that in two dimensions, the second effective deviatoric stress invariant is equal to the maximum shear stress and thus the failure mechanism predicted by this envelope would be shear, rather than purely tensile failure and, if the authors go this route, the authors will need to be careful to point this out. Although we speculated that shear failure is important for tall calving cliff in Bassis and Walker (2012), I'm not aware of any strong observational evidence supporting shear failure in calving so the authors may want to take this suggestion under advisement as the broader community has doubts about the viability of shear failure.*

As discussed in our response to point 1 above, this issue is avoided as a result of switching to use of the EPS stress metric.

**No changes were made in response to this specific comment. Changes already detailed in response to comment #1 remove the Vaughan (1993) tensile strength as a crevassing criterion, but it is still referenced in section 2.3 to justify our interpretation of the results.**

3. *Another minor point is that the authors convincingly argue that time scales they are interested are short compared to the time scales of flow and thus they can ignore the effect of ice flow on their experiments. However, if the time scale of interest is short compared to the time scale of flow, then this would seem to imply that an elastic rheology would be appropriate. This is surprising to most, but the elastic stress can be quite different from the viscous stress and this is primarily a consequence of the non-linearity in the creep flow law used.*

We are pleased that the reviewer finds our arguments regarding timescales convincing. We agree with this minor point that the stress should include an elastic component, though we suspect that the boundary conditions are the key factor, rather than nonlinearity. Here we have neglected elastic forces along the lines of (e.g. Benn et al., 2017; O'Leary and Christofferson, 2013) but accept that inclusion would change our results quantitatively. We do still expect a substantial increase in stress around the grounding line, since the force formerly acting on the bed downstream must be transferred upstream.

**No changes were made in response to this comment.**

4. *The authors should be a little bit careful when discussing sliding laws, water pressure and the stress regime because glaciers are actually three-dimensional with bumps in the bed. In three-dimensions, these bumps play a pretty big role in controlling the stress transmission*

*upstream because portions of the calving front maybe well grounded whilst other portions are close to flotation.*

**A new paragraph has been added at page 10, line 2 to communicate this point to the reader.**

### Additional changes

The authors made some minor further changes in order to correct minor mistakes, clarify meaning or improve the flow of the text, which were not based on recommendations by the reviewers.

- **Changed “mass balance of the Greenland Ice Sheet” to “Greenland Ice Sheet mass balance”, page 1 line 21.**
- **Added Greenlandic name of JI, page 1 line 24.**
- **Changed “superbuoyancy” to “super-buoyancy”, page 2 line 7.**
- **Added an extra final line to paragraph, page 2 line 13.**
- **Removed “further we”, page 2, line 25.**
- **Removed “however”, page 2, line 31.**
- **Added “when not present”, page 2 line 22.**
- **Added “applied here”, page 9 line 5.**
- **Changed “suggests” to “suggested”, page 9 line 9.**
- **Changed “trigger” to “induce”, page 9 line 16.**
- **For the sake of consistency, “basal drag” has been replaced with “basal shear stress” since these two terms were being used interchangeably. Changes made at page 4, line 9; page 4, line 15; page 5, line 27; page 7, line 31; page 9, line 4; page 9, line 28, table 1.**
- **Updated references to Cuffey and Patterson (2010) to account for differing page numbers.**
- **Updated figure 6 to match format of other figures. Figure content and caption unchanged.**
- **Added “The”, to the start of page 10, line 7.**
- **Changed “significantly” to “greatly” to enhance readability, page 10, line 26.**
- **Added “Code availability” section.**
- **Updated “Acknowledgements” section to clarify MT’s grant reference number.**
- **Corrected numerous typos in the references.**

# Buoyant forces promote tidewater glacier iceberg calving through large basal stress concentrations

Matt Trevers<sup>1</sup>, Antony J. Payne<sup>1</sup>, Stephen L. Cornford<sup>1,2</sup>, Twila Moon<sup>3</sup>

<sup>1</sup>Centre for Polar Observation and Modelling, School of Geographical Sciences, University of Bristol, Bristol, BS8 1SS, UK

5 <sup>2</sup>Department of Geography, Swansea University, Swansea, SA2 8PP, UK

<sup>3</sup>National Snow and Ice Data Center, University of Colorado, Boulder, CO 80309-0449 USA

*Correspondence to:* Matt Trevers (matt.trevers@bristol.ac.uk)

**Abstract.** Iceberg calving parameterisations currently implemented in ice sheet models do not reproduce the full observed range of calving behaviours. For example, though buoyant forces at the ice front are known to trigger full-depth calving events on major Greenland outlet glaciers, a multi-stage iceberg calving event at Jakobshavn Isbræ is unexplained by existing models. To explain this and similar events, we propose a notch-triggered rotation mechanism whereby a relatively small subaerial calving event triggers a larger full-depth calving event due to the abrupt increase in buoyant load and the associated stresses generated at the ice-bed interface. We investigate the notch-triggered rotation mechanism by applying a geometric perturbation to the subaerial section of the calving front in a diagnostic flowline model of an idealised glacier snout, using the full-Stokes, finite element method code Elmer/Ice. Different sliding laws and water pressure boundary conditions are applied at the ice-bed interface. Water pressure has a big influence on the likelihood of calving, and stress concentrations large enough to open crevasses were generated in basal ice. Significantly, the location of stress concentrations produced calving events of approximately the size observed, providing support for future application of the notch-triggered rotation mechanism in ice-sheet models.

## 20 1 Introduction

Iceberg calving from marine-terminating glaciers is an important component of the ~~mass balance of the~~ Greenland Ice Sheet mass balance. Calving accounted for a third of total mass loss between 2009 and 2012 (Enderlin et al., 2014). Moreover, calving is an important control on the flow dynamics of tidewater glaciers, reducing the backstress in the glacier snout region and leading to flow acceleration and dynamic thinning (Thomas, 2004). The acceleration of Jakobshavn Isbræ (JI, Sermeq Kujalleq in Greenlandic) by a factor of 4 since 1995, for example, is linked with its continued calving retreat following the disintegration of its ice shelf (Joughin et al., 2012).

Current models of iceberg calving fail to capture the full range of observed processes, and as such the parameterisations applied within ice sheet models are limited. van der Veen (1996) proposed the empirical height-above-flotation criterion, whereby the glacier calves to a point where its terminus is some fixed height above the flotation thickness. Although this method successfully reproduced advance and retreat behaviour for Columbia Glacier (Vieli et al., 2001) and Helheim Glacier

(Nick et al., 2009), a major shortcoming was the inability for ice to thin below the flotation thickness and form an ice tongue. A more physically based approach (Benn et al., 2007a, b) assumed that crevasses penetrating to the waterline penetrate through the full glacier thickness. This simple theory has been used in many recent modelling studies (e.g. Otero et al., 2010; Nick et al., 2013; Cook et al., 2014). However, since crevasse depths are calculated based on the equilibrium between  
5 longitudinal stretching and ice overburden pressure (Nye, 1957), calving in these models arises only as a result of ice flow dynamics. The effect of localised processes such as melt-water undercutting (Luckman et al., 2015) or ice-cliff collapse (Bassis and Walker, 2012), or of super-buoyancy upon near-terminus stresses is not captured in these models.

Buoyant forces have been proposed as a driver of large calving events observed at major Greenland Ice Sheet marine-terminating glaciers. Full-depth, ~~rotating slab~~bottom-out calving events observed at Helheim Glacier resulted from buoyant flexure of the glacier snout and the propagation of basal crevasses (e.g. Murray et al., 2015). Wagner et al. (2016) also showed that applying a buoyant force to an elastic beam model of a glacier resulted in large basal tensile stresses, which were further amplified by the emergence of a submarine protrusion of the calving face due to sea surface melting. Buoyant forces may be at play in driving as-yet unexplained calving styles.  
10

15 A multiple-iceberg calving event was observed at JI in August 2009 (Walter et al., 2012) that is not fully explained by existing calving models, but which we propose is tied to buoyant force changes over the course of the multi-stage calving event. In this observation, the collapse of a subaerial portion of the ice cliff was followed minutes later by a much larger, full-depth, bottom-out ~~rotating slab~~ calving event across the same section of the front. We consider a mechanism to explain  
20 this event whereby a substantial portion of the snout becomes buoyant immediately following a small subaerial calving event, which we term “notch-triggered rotation”. In this mechanism, visualised in Fig. 1, the sudden increase in buoyant load causes the snout to lift and rotate. The resultant basal tensile stresses initiate basal crevassing, which rapidly propagates through the full glacier thickness. This mechanism is similar to the “footloose” mechanism investigated by Wagner et al. (2014) and earlier proposed by Scambos et al. (2005) for the breakup of tabular icebergs. However, in this study we consider  
25 the very short timescales arising from abrupt changes in the geometry, and ~~further we~~ analyse the viscous stresses originating at the ice-bed interface rather than the elastic stresses resulting purely from bending.

Using a diagnostic numerical glacier model, we investigate whether notch-triggered rotation is a plausible calving mechanism. With sophisticated prognostic models, calving criteria can be tested by application to real glacier geometries  
30 (e.g. Nick et al., 2010; Krug et al., 2014) and the calving rate response to various environmental forcings can be quantified (e.g. Cook et al., 2014; Todd et al., 2014). Simpler diagnostic models, ~~however,~~ provide insight into iceberg calving mechanisms by resolving the internal stresses under instantaneously imposed geometries (e.g. Hanson and Hooke 2000, 2003; O’Leary and Christofferson, 2013). Here we use a diagnostic model that is able to quantify changes in the stress field induced by geometrical perturbations of the ice front.

## 2 Model setup

In this study we use a two-dimensional diagnostic flowline model of an idealised glacier snout, to determine whether the magnitude of stresses generated by the notch-triggered rotation mechanism is sufficient to result in calving. The mechanisms of crevasse propagation through the ice thickness are not examined. We apply the buoyant forcing in the model by cutting a notch into the subaerial ice cliff to a length  $l_n$  from the waterline to the surface (Fig. 2). The ice flow solution is calculated using the open source, full-Stokes, finite element Elmer/Ice modelling software (Gagliardini et al., 2013).

### 2.1 Ice flow model

Elmer/Ice calculates velocity and stress profiles within the glacier by solving the Stokes equations for an incompressible fluid (e.g. Gagliardini et al., 2013):

$$\nabla \cdot \mathbf{u} = 0 \quad (1)$$

$$\nabla \cdot \boldsymbol{\sigma} + \rho_i \mathbf{g} = \nabla \cdot \boldsymbol{\tau} - \nabla p + \rho_i \mathbf{g} = 0 \quad (2)$$

10 where  $\mathbf{u}$  is the velocity vector,  $\boldsymbol{\sigma}$  the Cauchy stress tensor,  $\rho_i = 918 \text{ kg m}^{-3}$  the ice density,  $\mathbf{g} = (0,0,-9.81) \text{ m s}^{-2}$  the acceleration due to gravity,  $\boldsymbol{\tau}$  the deviatoric stress tensor  $\boldsymbol{\tau} = \boldsymbol{\sigma} + p\mathbf{I}$ ,  $p$  the isotropic pressure  $p = -\text{tr}(\boldsymbol{\sigma})/3$  and  $\mathbf{I}$  the identity matrix,  $\rho_i = 918 \text{ kg m}^{-3}$  the ice density and  $\mathbf{g} = (0,0,-9.81) \text{ m s}^{-2}$  the acceleration due to gravity. The ice rheology is described using Glen's flow law which relates deviatoric stress to the strain rate  $(\dot{\epsilon}_{ij})$  (Glen, 1958):

$$\tau_{ij} = 2\mu\dot{\epsilon}_{ij} \quad (3)$$

The effective viscosity  $\mu$  is defined as

$$\mu = \frac{1}{2} A^{-1/n} \epsilon_e^{(1-n)/n} \quad (4)$$

15 where  $\epsilon_e^2$  is the square of the second invariant of the strain rate tensor and  $n = 3$  is the commonly used exponent in Glen's flow law. The Arrhenius factor  $A$  is expressed as

$$A = A_0 \exp(-Q/RT') \quad (5)$$

where  $A_0$  is a constant,  $Q$  the creep activation energy,  $R$  the universal gas constant and  $T'$  the temperature of ice relative to the pressure melting point (Cuffey and Patterson, 2010, p.64). For symbols and values used in this study, see Table 1. The temperature of glacier ice is set at a constant  $-9^\circ\text{C}$ .

20

### 2.2 Boundary conditions

We use typical boundary conditions for a tidewater glacier. Along the upper surface, as well as the rear and lower surfaces delineating the notch when one is present, or the subaerial portion of the ice front ~~otherwise when not present~~, we ignore atmospheric pressure and apply a stress-free boundary condition:

$$\sigma_{nn} = 0 \quad (6)$$

$$\sigma_{nt} = 0$$

where  ~~$\sigma$  is the Cauchy stress and~~ subscripts  $n$  and  $t$  refer to normal and tangential directions. Hydrostatic pressure is applied at the ice front below the waterline:

$$p_w = -\rho_w g z \quad (7)$$

where  $p_w$  is the water pressure,  $\rho_w = 1028 \text{ kg m}^{-3}$  the ice density and the vertical  $z$  axis is centred at the waterline. At the rear boundary 10 km upstream, lithostatic pressure is applied along with an inflow velocity of  $5000 \text{ m a}^{-1}$ , chosen to roughly match the flow speed of JI at a similar distance from the calving front (Vieli and Nick, 2011).

At the basal boundary, a choice of sliding laws was available for grounded ice. ~~Weertman-type power laws~~The Weertman law (Weertman, 1957) ~~are commonly used~~ in glacier modelling applications (e.g. Krug et al., 2014; Cornford et al., 2015). ~~This law~~ takes the form:

$$\tau_b = C |u|^{m-1} u \quad (8)$$

with  $\tau_b$  the basal ~~drag~~shear stress,  $C$  the Weertman friction coefficient and sliding exponent  $m = 1/3$ . Values of  $C$  range from  $10^5$  to  $10^8 \text{ Pa m}^{-1/3} \text{ s}^{1/3}$ , which includes the more realistic range of modelled values of  $\sim 10^6$  to  $\sim 10^7 \text{ Pa m}^{-1/3} \text{ s}^{1/3}$  determined from surface velocity observations around Greenland outlet glaciers (Lee et al., 2015).

Alternatively, a Coulomb-limited sliding law (Schoof, 2005; Gagliardini et al., 2007) can be applied (referred to as the “Schoof law” from here on in). This law accounts for the effect of water pressure through an effective pressure term  $N = -\sigma_{nn} - P_w$ . Basal ~~drag~~shear stress is expressed as

$$\tau_b = C_c \cdot N \left( \frac{\chi}{1 + \alpha \chi^q} \right)^{1/n} \quad (9)$$

where

$$\chi = \frac{u}{C_c^n N^n A_s} \quad (10)$$

and

$$\alpha = \frac{(q-1)^{q-1}}{q^q}. \quad (11)$$

$C_c = 1$  is the maximum value of  $\tau_b/N$ ,  $q = 1$  is the post-peak exponent,  $A_s$  is the value of the sliding coefficient in the absence of cavitation and  $n$  is the flow law exponent. As in previous studies (e.g. Nick et al., 2010; Krug et al., 2014) a free hydrological connection is assumed between the subglacial drainage system and the sea, so hydrostatic water pressure is applied at the ice-bed interface.

The contact problem (Durand et al., 2009) is solved at the ice-bed interface to determine where ice is grounded or floating. In this implementation, nodes touching the bedrock where the normal stress exerted by the ice is greater than the seawater pressure ( $\sigma_{nn} > p_w(z_b)$ ) are considered grounded and have zero vertical velocity, while nodes that have separated from the

bedrock or where  $\sigma_{nn} \leq p_w(z_b)$  are floating and can have non-zero vertical velocity. The model is initialised with the glacier fully grounded along its entire length.

### 2.3 Stress analysis

5 As in other studies (e.g. Nick et al., 2010; Todd et al., 2014), we assess the likelihood of crevasse opening from the magnitude of the resulting stress distribution. The largest principal Cauchy stress  $\sigma_1$  is coordinate system invariant, accounting for crevasse opening in any direction:

$$\sigma_1 = \frac{\sigma_{xx} + \sigma_{zz}}{2} + \sqrt{\left(\frac{\sigma_{xx} - \sigma_{zz}}{2}\right)^2 + \sigma_{xz}^2} \quad (12)$$

Because the overburden pressure beneath a kilometre-thick column of ice is in the order of 10 MPa,  $\sigma_1$  is negative almost everywhere at depth. Following Benn et al. (2017), we superpose the hydrostatic water pressure to define the effective principal stress (EPS):

$$\text{EPS} = \sigma_1 + p_w \quad (13)$$

10 The hydrostatic pressure is similar in magnitude to the ice overburden pressure at the glacier bed.

In previous modelling studies (e.g. Otero et al., 2010; Cook et al., 2012), crevasses were assumed to exist in regions of the glacier where the stress is tensile ( $\sigma > 0$ ), following the method proposed by Nye (1957). Schulson (2001) suggests a fracture strength of 0.8 MPa for polycrystalline ice at -10 °C with a grain size of 10 mm, with decreasing strength for increasing grain  
 15 size. Vaughan (1993) estimated tensile strength between 0.09 MPa and 0.32 MPa by fitting a von Mises failure envelope to field observations of crevassed and uncrevassed regions. In this study we do not calculate crevasse penetration heights, therefore we do not apply a crevassing or calving criterion. Instead, we infer the existence of crevasses where the EPS is of a similar magnitude to these estimates (~0.5 MPa).

### **3 Model Results**

20 Experiments were run for a glacier with water depth  $d_w = 900$  m, terminus thickness  $h_t = 980$  m, surface slope  $\alpha = 3^\circ$  and  $C = 2.371 \times 10^6 \text{ Pa m}^{-1/3} \text{ s}^{1/3}$ , with notches cut to varying lengths. For these experiments, full hydrostatic pressure (Eq. 7) was applied along the basal boundary. Figure 4 shows ~~longitudinal deviatoric stresses  $\tau_{xx}$~~  EPS mapped for the  $l_n = 100$  m case, with the  $l_n = 0$  m case mapped in Fig. 3 for comparison. Basal stresses are plotted for  $l_n = 0$  m,  $l_n = 80$  m and  $l_n = 100$  m (Fig. 5). ~~An estimate of the tensile strength of glacier ice from Vaughan (1993) is also plotted to provide estimates of the critical~~  
 25 ~~stress required for basal crevasse opening.~~

Notch cutting caused basal ice to become ungrounded between approximately 494-190 m and 644-640 m upstream of the ice front for  $l_n = 100$  m (Fig. 4). Prominent stress concentrations associated with ungrounding and regrounding also appeared at

the basal boundary which were not present in the unperturbed case. ~~These stresses exceed the tensile strength of ice and would therefore result in crevasse initiation.~~ The tensile ~~stress stress~~ peak centred ~~around approximately 644-640~~ m upstream of the ice front resulted from separation of basal ice from the bedrock, as the buoyant snout tended to lift. The abrupt change in basal ~~drag shear stress~~ across the grounding zone, where ice that has separated from the bedrock accelerates, gave rise to this stress peak. Further notch-cutting caused this stress peak to shift upstream and increase in magnitude. The substantial growth in concentrated stress at this location to approximately 1.4 MPa would likely result in crevasse opening.

The region of compressive stress centred ~~around approximately 191-190~~ m upstream of the ice front arose from ice regrounding on the bedrock downstream of the grounding line, due to the backstress applied on the ice front by hydrostatic pressure. An imbalance between the hydrostatic and cryostatic pressure normal to the terminus tends to warp the snout downwards (see Fig. S1; Reeh, 1968), with the same effect seen at the start of prognostic model runs by Benn et al. (2017). Experiments in which the hydrostatic pressure from the pro-glacial water body was removed, or the bedrock lowered downstream of the grounding line, did not include this compressive stress peak while still featuring the tensile stress peak, supporting our assertion that the compressive stress concentration resulted from basal ice regrounding.

Corresponding longitudinal velocity maps for the frontal region are shown in Fig. S2 (unperturbed) and Fig. S3 ( $l_n = 100$  m). There is an acceleration of  $\sim 2000$  m a<sup>-1</sup> following the notch cutting, resulting from the reduced basal friction in the ungrounded region.

A critical notch length  $l_{crit}$  was required before the glacier snout became buoyant and the tensile stress peak appeared. A sensitivity study was carried out to explore the relationship of this critical notch length to the bed stickiness and the glacier surface slope (Fig. 6), and to determine how this relationship affects the maximum basal stress (Fig. 7). Setting the notch length  $l_n = l_{crit}$  resulted in a noisy maximum basal stress signal so we instead set  $l_n = l_{crit} + 25$  m which allows a coherent pattern to emerge.

Ungrounding occurred even without a notch on glaciers with very slippery beds for all surface slopes, and at all values of the friction coefficient for a 2° surface slope. For steeper surface slopes the critical notch length increased with bed stickiness before levelling off. For a given value of the friction coefficient, the critical notch length also increased with surface slope. Similarly, the maximum basal stress increased with both friction coefficient and surface slope. For very slippery beds the maximum stress was below the upper boundary of the tensile strength envelope, but significantly it was above the critical stress for crevasse initiation through the realistic range of friction coefficients  $C = 10^6$  to  $10^7$  Pa m<sup>-1/3</sup> s<sup>1/3</sup>.

These experiments reveal a complex picture of the conditions that favour calving. An explanation for the relationship between the critical notch length and bed stickiness does not readily present itself, and this effect may warrant further

investigation. The relationships of surface slope with both the critical notch length and the maximum basal stress are more easily explained. The terminus of a steeper sloped glacier is more strongly grounded, requiring the removal of more ice to render it buoyant, than a more gently sloping glacier. The longer submarine foot and larger buoyant forces that result then favour larger basal stresses (e.g. Wagner et al., 2016).

### 5 3.1 Water pressure dependency

Tidewater glaciers such as JI are subject to the influence of water pressure where they meet the ocean, therefore it is appropriate to examine the region around the grounding line and calving front using a water pressure-dependent sliding law.

Since the large basal stresses were generated by the abrupt change in basal shear stress across the grounding line, a sliding law in which the basal shear stress reduces gradually as a function of effective pressure would not be expected to produce

10 such large stress concentrations. To investigate the effects of water pressure upon the notch-triggered rotation mechanism, experiments were conducted using the Schoof law (Eq. 9). In all following experiments a similar setup as before was used, with  $\alpha = 3^\circ$ , a varying notch length, and the sliding coefficient  $A_s = 3.169 \times 10^{-21} \text{ Pa}^{-3} \text{ m s}^{-1}$ . Experiments F0 and F100 were carried out with full hydraulic connectivity at the ice-bed interface, and experiments Z0 and Z100 with zero hydraulic connectivity (i.e.  $p_w = 0$  everywhere). See Table 2 for details of parameters used in Schoof law experiments.

15

The resulting stress profiles for these experiments (~~Fig. 8~~) are highly dependent on the basal water pressure, ~~with~~ Experiments Z0 and Z100 (Fig. 8) exhibiting exhibited stress patterns identical-very similar to those produced by the Weertman law experiments, although the stress is compressive everywhere due to the exclusion of water pressure, inhibiting any possibility of crevasses opening.

20 large tensile stress that exists independent of any perturbation. Notch cutting has minimal impact on the magnitude or location of this region. This region of large stress exists because the basal shear stress in the frontal region is small, since the effective pressure is zero; therefore, the basal shear stress is increased upstream, and this upstream transfer of stress occurs via a region of increased englacial tensile stress. The magnitude of these stresses suggests an inherent instability for glaciers in such a configuration when subject to full basal water pressure.

25

The assumption of perfect hydraulic connectivity, however, may not hold for large distances upstream of the grounding line (Cuffey and Paterson, 2010, p. 283). We therefore carried out additional experiments P0 and P100 (Fig. 10) to simulate limited hydraulic connectivity by linearly reducing the water pressure at the ice-bed interface from full hydrostatic pressure at the front to zero at the rear of the domain (Table 2), similarly to Leguy et al. (2014). Experiment P0 shows a region of large tensile stress, ~~like similar to but smaller than~~ those seen in experiments F0 and F100 (~~Fig. 9~~). The notch perturbation in experiment P100 results in a ~~Weertman like~~ stress peak similar to those produced by the Weertman law which is significantly larger in magnitude than the unperturbed stress peak.

30

## 4 Discussion

Our experiments show that perturbations to the ice front geometry can induce large stress concentrations in basal ice. The magnitude and location of these stress concentrations shows a strong dependency on the basal ~~drag~~shear stress. For a glacier snout already close to flotation, only a relatively small perturbation was required to induce large stresses. This is in line with the observed relationship between calving rate and water depth (Brown et al., 1982).

The large internal stress concentrations reported here are attributed to the requirement to balance the abrupt decrease in basal shear stress across the grounding line and are not associated with bending stresses. This distinction is based on the following observations. Firstly, the region of additional high stress is sharply focused at the glacier bed and is not balanced by a region of compressive stress at the surface as would be expected for a viscous bending moment (Mosbeux et al., 2019). Secondly, the stress concentration is compressive where the ice regrounds further downstream, whereas a bending stress at this location would also be tensile. Finally, we have shown that the form and magnitude of stress is highly dependent upon the choice of sliding law and application of basal water pressure, which would be largely irrelevant for bending stresses.

The choice of diagnostic model for a calving study was criticised by Cook et al. (2014) after their prognostic model showed much greater sensitivity to atmospheric as opposed to oceanic forcing than diagnostic models (O’Leary and Christoffersen, 2013), suggesting that this was due to the inability of a diagnostic model to respond to stress perturbations through ice deformation. However, over the short timescales of interest in this study, deformation of ice is negligible. In our experiments, measured vertical velocities for the ungrounded regions of basal ice were of the order  $\sim 10 \text{ m a}^{-1}$ , equating to  $\sim 0.1 \text{ mm}$  of lifting over 5 minutes, which would have negligible effect on the stress field. Therefore, our choice of a diagnostic model is an appropriate one for this study.

As in other diagnostic studies we did not apply a calving criterion, instead using the location of basal stress peaks as an indication of where crevasses may form. For this to result in calving on the timescale proposed requires the assumption of full-thickness crevassing on timescales much faster than those observed by e.g. Murray et al. (2015). Given a sufficiently large buoyancy force, this assumption can be held as true, as once a crack has initiated, the tensile stress which opened that crack refocuses at the crack tip causing it to continue to propagate. As the crevasse increases in height, hydrostatic pressure acting to open the crevasse decreases at a faster rate than the ice overburden pressure acting to close it; therefore, larger basal stresses are required for full-depth crevassing than for crevasse initiation. However, once a crevasse has started to propagate and the downstream portion of the snout has begun to lift and rotate, elastic stresses further contribute to the crevasse growth in a feedback process. Benn et al. (2017) reported that glacier geometries that did not result in calving in Elmer/Ice via crevasse depth calving laws still produced large full-depth calving event when exported into HiDEM, a model representing glacier ice as a lattice of particles connected by breakable elastic beams. Further investigation of the rate and modes of

crevasse propagation could integrate Linear Elastic Fracture Mechanics into a glacier model featuring basal crevasses (van der Veen, 1998), or use a model such as HiDEM in conjunction with Elmer/Ice (Benn et al., 2017).

5 Our study builds on that of O’Leary and Christoffersen (2013), which also explored the effect of geometrical perturbations at the ice front on the likelihood of calving. Their study found that undercutting led to larger calving events and a higher overall calving rate, which appears to be at odds with the results presented here: undercutting would reduce the buoyant load and potentially stabilise the terminus. Our results differ because the sharp transition in basal ~~drag-shear stress~~ is not possible at the stress-free surface boundary applied here. Furthermore, the geometry of their model was set up to explore surface crevassing while ours was designed to explore basal crevassing. In reality a mixture of these effects may be working together  
10 to promote or prohibit calving.

Figure 1 suggest~~ed~~ the subaerial calving event may result from undercutting by a waterline notch. Although this process is observed at some glaciers (e.g. Kirkbride and Warren, 1997; Röhl, 2006) it is questionable whether it could be a major factor in the Ilulissat Icefjord (where the original observation was made), in which the loosely bonded mélange in summer may act  
15 to damp any wavecutting action (Amundson et al., 2010). An alternative potential mechanism for triggering the subaerial calving event is provided by spontaneous collapse of the ice cliff. The maximum stable cliff height for damaged glacier ice was calculated by Bassis and Walker (2012) as 110 m while Hanson and Hooke (2003) suggested a maximum stable height of ~ 70 m based on diagnostic model experiments. The ice cliffs of JI approach 100 m but rarely exceed this height, suggesting that the inherent instability of ice cliffs may be the limiting factor and could ~~trigger-induce~~ calving through notch-  
20 triggered rotation.

Buoyancy in a glacier snout can also be induced by thinning due to high surface melt rates. However, the almost immediate increase of buoyant load resulting from the subaerial calving event proposed here occurs on timescales much faster than can be accommodated by ice creep, leading to a higher probability of calving (e.g. Boyce et al., 2007). The specific location of  
25 the basal stress peak varied with many parameters including the notch length but tended to be within one ice thickness of the terminus, consistent with observations (e.g. Walter et al., 2012, Murray et al., 2015). The location of the peak stress always occurred much further back from the terminus than the cliff at the rear of the notch, leading to an amplification of the original subaerial calving event. The value of this amplifying factor cannot be accurately quantified within the limitations of a diagnostic model; however, it may present a method of linking environmental forcings to the calving rate.

30 There are a number of possible refinements to our model. We ignored lateral drag, which combines with basal ~~drag-shear stress~~ to support the driving stress. Although lateral drag may be negligible along the flowline of wide ice streams, JI was able to form a floating tongue so it must be assumed that lateral drag is significant (e.g. Thomas, 2004). Its omission may have caused the model to overstate the dependence of basal stresses on the basal sliding law. Our model also omits the effect

of temperature. The viscosity of ice and transmission of stresses are dependent on thermal gradients. JI has large vertical temperature gradients (Lüthi et al., 2002) and temperate basal ice, which are thought to play a role in its fast sliding. Warmer basal temperatures may act to damp the intensity of basal stress concentrations.

5 The reader should note that our model geometry is idealised. In reality, glacier beds are highly non-uniform, with variations in geometry, water and overburden pressure across a range of spatial and temporal scales. Bedrock bumps therefore play an important role in controlling the stress transmission upstream. It is plausible that these variations could result in basal stress concentrations of a similar magnitude to the mechanism discussed here.

10 ~~Note~~The notch-triggered rotation mechanism was shown to be irrelevant ~~under the full Schoof regime~~when using the Schoof law with full water pressure, since a glacier in these conditions would tend to be vulnerable to buoyant calving anyway. This raises the question of whether the Schoof law with full water pressure provides an accurate representation of basal sliding for JI. We expect low effective pressure in the frontal region, however given that the glacier snout is mostly grounded in the summer (e.g. Amundson et al, 2010), perfect hydraulic connectivity cannot be assumed along the ice-bed interface. Complete suppression of water pressure at the ice-bed interface resulted in a basal stress pattern ~~identical~~very similar to the Weertman case, although strongly compressive everywhere due to the exclusion of water pressure in the calculation of EPS, and therefore very unlikely to result in crevassing. With  $C_c = q = 1$  and  $m = 1/n$  as in this study, it can be easily shown that large  $N$  (~10 MPa in the absence of water pressure) leads to small  $\chi$  and Eq. (9) reduces to a Weertman power law:

$$\tau_b = (u_b A_s^{-1})^{1/n}. \quad (4214)$$

20

On the other hand, limiting the basal water pressure without suppressing it completely (experiments P0 and P100) resulted in a transition case displaying similar behaviour ~~from to~~ both the Weertman and Schoof ~~regimes~~laws; the unperturbed stress profile was similar to ~~that produced by the~~ Schoof ~~law~~case, but the perturbation resulted in a significantly larger ~~Weertman-like~~ stress peak like those produced by the Weertman law. This raises the possibility that a lightly grounded glacier snout, already in a state of basal tension, could be subjected to high enough stress by a minor subaerial calving event, like that observed at JI (Walter et al., 2012), to cause full depth crevassing and buoyant calving.

25

## 5 Conclusions

Our results show that the notch-triggered rotation mechanism does produce calving for an idealized marine-terminating glacier. Although notch-triggered rotation did not significantly affect stresses when applying the Schoof law under full hydrostatic pressure, removing the assumption of perfect hydraulic connectivity at the ice-bed interface ~~significantly~~greatly enhanced the likelihood of calving through this mechanism. Significantly, a realistic length scale for calving events, on the

30

order of hundreds of meters and generally less than one ice thickness, naturally results from the model physics. Fast flowing glaciers near flotation and with shallow surface slopes may be especially vulnerable to buoyant calving due to basal crevassing. The notch-triggered rotation mechanism proposed here to explain the observed calving event (Walter et al., 2012) does not replace other models of calving. Instead, it bolsters our understanding of calving by providing insight into multi-stage calving events occurring particularly on large, fast-flowing tidewater glaciers.

### **Code availability**

Elmer/Ice code is publicly available through GitHub (<https://github.com/ElmerCSC/elmerfem>). All simulations were performed with version 8.3 of Elmer/Ice. All scripts used for simulations are available upon request from authors.

### **Author contribution**

10 M.T. designed the experiments with contributions from A.J.P. and S.L.C and M.T. carried them out. M.T. prepared the manuscript with contributions from all co-authors.

### **Competing interests**

The authors declare that they have no conflict of interest.

### **Acknowledgements**

15 M.T. is supported by a NERC GW4+ Doctoral Training Partnership studentship from the Natural Environment Research Council [NE/L002434/1]. ~~was supported by the Natural Environment Research Council (NERC) through the Great Western~~  
~~Four+ (GW4+) Doctoral Training Partnership.~~ We thank Olivier Gagliardini and Thomas Zwinger for running the free Elmer/Ice training course at the Neils Bohr Institute, Copenhagen in November 2015. We thank Olivier Gagliardini in particular for suggestions on the study scope and invaluable technical support. We also thank Till Wagner for useful  
20 comments on the original manuscript.

### **References**

Amundson, J. M., Fahnestock, M., Truffer, M., Brown, J., Lüthi, M. P., and Motyka, R. J.: Ice mélange dynamics and implications for terminus stability, Jakobshavn Isbræ, Greenland, J. Geophys. Res., 115, F01005, <https://doi.org/10.1029/2009JF001405>, 2010.

- Bassis, J. N. and Walker, C. C.: Upper and lower limits on the stability of calving glaciers from the yield strength envelope of ice, *P. Roy. Soc. Lond. A Mat.*, 468, 913–931, <https://doi.org/10.1098/rspa.2011.0422>, 2012.
- Benn, D. I., Hulton, N. R., and Mottram, R. H.: ‘Calving laws’, ‘sliding laws’ and the stability of tidewater glaciers, *Ann. Glaciol.*, 46, 123–130, 2007a.
- 5 Benn, D. I., Warren, C. R., and Mottram, R. H.: Calving processes and the dynamics of calving glaciers, *Earth-Sci. Rev.*, 82, 143–179, <https://doi.org/10.1016/j.earscirev.2007.02.002>, 2007b
- Benn, D. I., Aström, J., Todd, J., Nick, F. M., Hulton, N. R., and Luckman, A.: Melt-undercutting and buoyancy-driven calving from tidewater glaciers: new insights from discrete element and continuum model simulations, *J. Glaciol.*, 63, 691–702, 2017.
- 10 Boyce, E. S., Motyka, R. J. and Truffer, M.: Flotation and retreat of a lake-calving terminus, Mendenhall Glacier, southeast Alaska, USA, *Journal of Glaciology*, 53, 211–224, doi:10.3189/172756507782202928, 2007
- Brown, C. S., Meier, M. F. and Post, A.: Calving speed of Alaska tidewater Glaciers, with application to Columbia Glacier, U.S. Geological Survey Professional Paper, 1258–C, 1982.
- [Cook, S., Zwinger, T., Rutt, I. C., O’Neel, S., and Murray, T.: Testing the effect of water in crevasses on a physically based calving model, \*Ann. Glaciol.\*, 53, 90–96, https://doi.org/10.3189/2012AoG60A107, 2012](https://doi.org/10.3189/2012AoG60A107)
- 15 [Cook, S., Rutt, I. C., Murray, T., Luckman, A., Zwinger, T., Selmes, N., Goldsack, A. and James, T. D.: Modelling environmental influences on calving at Helheim Glacier in eastern Greenland, \*The Cryosphere\*, 8, 827–841, doi: 10.5194/tc-8-827-2014, 2014.](https://doi.org/10.5194/tc-8-827-2014)
- Cuffey, K. and Paterson, W. S. B.: *The Physics of Glaciers*, Academic Press, ~~p. 283~~, 2010
- 20 Durand, G., Gagliardini, O., De Fleurian, B., Zwinger, T. and Le Meur, E.: Marine ice sheet dynamics: Hysteresis and neutral equilibrium, *Journal of Geophysical Research: Solid Earth*, 114, 1–10, doi:10.1029/2008JF001170, 2009.
- Enderlin, E. M., Howat, I. M., and Vieli, A.: High sensitivity of tidewater outlet glacier dynamics to shape, *The Cryosphere*, 7, 1007–1015, doi:10.5194/tc-7-1007-2013, 2014.
- Gagliardini, O., Zwinger, T., Gillet-Chaulet, F., Durand, G., Favier, L., De Fleurian, B., Greve, R., Malinen, M., Martín, C., 25 Råback, P., Ruokolainen, J., Sacchetti, M., Schäfer, M., Seddik, H. and Thies, J.: Capabilities and performance of Elmer/Ice, a new-generation ice sheet model, *Geoscientific Model Development*, 6, 1299–1318, doi:10.5194/gmd-6-1299-2013, 2013.
- [Glen, J. W.: The flow law of ice. A discussion of the assumptions made in glacier theory, their experimental foundations and consequences, \*Int. Assoc. Sci. Hydrol.\*, 47, 171–183, 1958.](https://doi.org/10.1002/hyp.650)
- 30 Hanson, B. and Hooke, R. L.: Glacier calving: a numerical model of forces in the calving-speed/water-depth relation, *J. Glaciol.*, 46, 188–196, 2000.
- Hanson, B. and Hooke, R. L.: Buckling rate and overhang development at a calving face, *J. Glaciol.*, 49, 577–586, 2003.

- Joughin, I., Smith, B. E., Howat, I. M., Floricioiu, D., Alley, R. B., Truffer M. and Fahnestock, M. A.: Seasonal to decadal scale variations in the surface velocity of Jakobshavn Isbræ, Greenland: Observation and model-based analysis, *Journal of Geophysical Research: Earth Surface*, 117, 1-20, doi:10.1029/2011JF002110, 2012.
- Kirkbride, M. P. and Warren, C. R.: Calving processes at a grounded ice cliff, *Ann. Glaciol.*, 24, 116–121, 1997.
- 5 Krug, J., Weiss, J., Gagliardini, O., and Durand, G.: Combin—ing damage and fracture mechanics to model calving, *The Cryosphere*, 8, 2101–2117, <https://doi.org/10.5194/tc-8-2101-2014>, 2014.
- Lee, V., Cornford, S. L. and Payne, A. J.: Initialization of an ice-sheet model for present-day Greenland, *Annals of Glaciology*, 56, 129-140, doi:10.3189/2015AoG70A121, 2015.
- Leguy, G. R., Asay-Davis, X. S., and Lipscomb, W. H.: Parameterization of basal friction near grounding lines in a one-  
10 dimensional ice sheet model, *The Cryosphere*, 8, 1239–1259, doi:10.5194/tc-8-1239-2014, <http://www.the-cryosphere.net/8/1239/2014/>, 2014.
- Luckman, A., Benn, D. I., Cottier, F., Bevan, S., Nilsen, F., and Inall, M.: Calving rates at tidewater glaciers vary strongly with ocean temperature, *Nat. Commun.*, 6, 8566, <https://doi.org/10.1038/ncomms9566>, 2015.
- Lüthi, M. P., Funk, M., Iken, A., Gogineni, S. and Truffer, M.: Mechanisms of fast flow in Jakobshavn Isbrae, West  
15 Greenland: Part III. Measurements of ice deformation, temperature and cross-borehole conductivity\_in boreholes to the bedrock, *Journal of Glaciology*, 48, 369-385, doi:10.3189/172756502781831322, 2002.
- [Mosbeux, C., Wagner, T., Becker, M., and Fricker, H. A.: Viscous and elastic buoyancy stresses as drivers of ice-shelf calving, in preparation, 2019\[MT1\].](#)
- Murray, T., Selmes, N., James, T. D., Edwards, S., Martin, I., O'Farrell, T., Aspey, R., Rutt, I., Nettles, M. and Baugé, T.:  
20 Dynamics of glacier calving at the ungrounded margin of Helheim Glacier, southeast Greenland, *Journal of Geophysical Research: Earth Surface*, 120, 964–982, doi:10.1002/2015JF003531, 2015.
- Nick, F. M., Vieli, A., Howat, I. M., and Joughin, I.: Large-scale changes in Greenland outlet glacier dynam—ics triggered at the terminus, *Nat. Geosci.*, 2, 110–114, <https://doi.org/10.1038/ngeo394>, 2009.
- Nick, F. M., van der Veen, C. J., Vieli, A. and Benn, D. I.: A physically based calving model applied to marine outlet  
25 glaciers and implications for the glacier dynamics, *Journal of Glaciology*, 56, 781–794, doi:10.3189/002214310794457344, 2010.
- Nick, F., ~~Vieli, A.~~ Vieli, A., Andersen, M. L., Joughin, I., Payne, A., Edwards, T., Pattyn, F., and van de Wal, R.: Future sea-level rise from Greenland's main outlet glaciers in a warming climate, *Nature*, 479, 235–238, <https://doi.org/10.1038/nature12068>, 2013.
- 30 Nye, J. F.: The distribution of stress and velocity in glaciers and ice-sheets, *P. Roy. Soc. Lond. A Mat.*, 239, 113–133, 1957.
- O'Leary, M. and Christoffersen, P.: Calving on tidewater glaciers amplified by submarine frontal melting, *The Cryosphere*, 7, 119–128, doi:10.5194/tc-7-119-2013, 2013.

- Otero, J., Navarro, F., Martin, C., Cuadrado, M., and Corcuera, M.: A three-dimensional calving model: numerical experiments on Johnsons Glacier, Livingston Island, Antarctica, *J. Glaciol.*, 56, 200–214, <https://doi.org/10.3189/002214310791968539>, 2010.
- Reeh, N.: On the calving of ice from floating glaciers and ice shelves, *Journal of Glaciology*, 7, 215–232, doi: 10.3198/1968JoG7-50-215-232, 1968.
- Röhl, K.: Thermo-erosional notch development at fresh-water calving Tasman Glacier, New Zealand, *J. Glaciol.*, 52, 203–213, 2006.
- Scambos, T., Sergienko, O., Sargent, A., McAyeal, D., and Fastook, J.: ICESat profiles of tabular iceberg margins and iceberg breakup at low latitudes, *Geophys. Res. Lett.*, 32, <https://doi.org/10.1029/2005GL023802>, 2005.
- Schoof, C.: The effect of cavitation on glacier sliding, *P. Roy. Soc. A-Math. Phys.*, 461, 609–627, <https://doi.org/10.1098/rspa.2004.1350>, 2005.
- [Schulson, E. M.: Brittle failure of ice. \*Eng. Fract. Mech.\*, 68, 1839–1887, doi:10.1016/S0013-7944\(01\)00037-6, 2001.](https://doi.org/10.1016/S0013-7944(01)00037-6)
- Thomas, R. H.: Force-perturbation analysis of recent thinning and acceleration of Jakobshavn Isbræ, Greenland, *J. Glaciol.*, 50, 57–66, doi:10.3189/172756504781830321, 2004
- Todd, J. and Christoffersen, P.: Are seasonal calving dynamics forced by buttressing from ice mélange or undercutting by melting? Outcomes from full-Stokes simulations of Store Gletscher, West Greenland. *The Cryosphere*, 8, 2353–2365, doi:10.5194/tc-8-2353-2014, 2014.
- van der Veen, C. J.: Tidewater calving, *J. Glaciol.*, 42, 375–385, 1996.
- van der Veen, C. J.: Fracture mechanics approach to penetration of bottom crevasses on glaciers, *Cold Regions Science and Technology*, 27, 213–223, doi:10.1016/S0165-232X(98)00006-8, 1998.
- Vaughan, D. G.: Relating the occurrence of crevasses to surface strain rates, *Journal of Glaciology*, 39, 255–266, doi:10.1016/0148-9062(94)90888-5, 1993.
- Vieli, A., Funk, M., and Blatter, H.: Flow dynamics of tidewater glaciers: a numerical modelling approach, *J. Glaciol.*, 47, 595–606, 2001.
- Vieli, A. and Nick, F. M.: Understanding and Modelling Rapid Dynamic Changes of Tidewater Outlet Glaciers: Issues and Implications. *Surveys in Geophysics*, 32, 437–458, doi: 10.1007/s10712-011-9132-4, 2011.
- Wagner, T. J. W., Wadhams, P., Bates, R., Elosegui, P., Stern, A., Vella, D., Abrahamsen, E. P., Crawford, A., and Nicholls, K. W.: The footloose mechanism: Iceberg decay from hydrostatic stresses, *Geophys. Res. Lett.*, 41, 5522–5529, 2014.
- Wagner, T. J. W., James, T. D., Murray, T. and Vella, D.: On the role of buoyant flexure in glacier calving, *Geophysical Research Letters*, 43, 232–240, doi:10.1002/2015GL067247, 2016.
- Walter, F., Amundson, J. M., O'Neel, S., Truffer, M., Fahnestock, M. A. and Fricker, H. A.: Analysis of low-frequency seismic signals generated during a multiple-iceberg calving event at Jakobshavn Isbræ, Greenland, *Journal of Geophysical Research: Earth Surface*, 117, 1–11, doi:10.1029/2011JF002132, 2012.
- [Weertman, J.: On the sliding of glaciers. \*J. Glaciol.\* 3, 33–38, 1957.](https://doi.org/10.1016/S0013-7944(01)00037-6)

5

10

15

20

25

Parameter	Symbol	Value	Units
Arrhenius factor	$A$		$\text{Pa}^{-3} \text{s}^{-1}$
Coulomb sliding coefficient	$A_s$	$3.169 \times 10^{-21}$	$\text{Pa}^{-3} \text{m s}^{-1}$
Arrhenius prefactor	$A_0$	1916	$\text{Pa}^{-3} \text{s}^{-1}$
Weertman friction coefficient	$C$	$10^5 - 10^8$	$\text{Pa m}^{-1/3} \text{s}^{-1/3}$

Maximum value of $\tau_b/N$	$C_c$	1	
Water depth	$d_w$	900	m
<u>Effective principal stress</u>	<u>EPS</u>		<u>Pa</u>
Acceleration due to gravity	$g$	9.81	$\text{m s}^{-2}$
Terminus thickness	$h_t$	980	m
<u>Identity matrix</u>	<u>I</u>		
Critical notch length	$l_{\text{crit}}$		m
Notch length	$l_n$		m
Weertman sliding exponent	$m$	1/3	
Effective pressure	$N$		Pa
Glen's flow law exponent	$n$	3	
Pressure tensor	$\boldsymbol{p}$		Pa
Water pressure	$p_w$		Pa
Post-peak exponent	$q$	1	
Creep activation energy	$Q$	139	$\text{kJ mol}^{-1}$
Universal gas constant	$R$	8.314	$\text{J K}^{-1} \text{mol}^{-1}$
Pressure-adjusted temperature	$T'$		K
Velocity tensor	$\boldsymbol{u}$		$\text{m s}^{-1}$
Glacier surface gradient	$\alpha$	2 – 5	°
Strain rate tensor	$\dot{\boldsymbol{\epsilon}}$		$\text{s}^{-1}$
Square of 2 <sup>nd</sup> invariant of $\dot{\boldsymbol{\epsilon}}$	$\dot{\boldsymbol{\epsilon}}_e^2$		$\text{s}^{-2}$
Effective viscosity	$\mu$		Pa s
Ice density	$\rho_i$	918	$\text{kg m}^{-3}$
Water density	$\rho_w$	1028	$\text{kg m}^{-3}$
Cauchy stress tensor	$\boldsymbol{\sigma}$		Pa
<u>Largest principal Cauchy stress</u>	<u><math>\sigma_1</math></u>		<u>Pa</u>
Deviatoric stress tensor	$\boldsymbol{\tau}$		Pa

Basal ~~drag~~shear stress

$\tau_b$

Pa

**Table 1. Symbols and values of physical and numerical constants and parameters used in this study.**

5

10

15

20

25

30

---

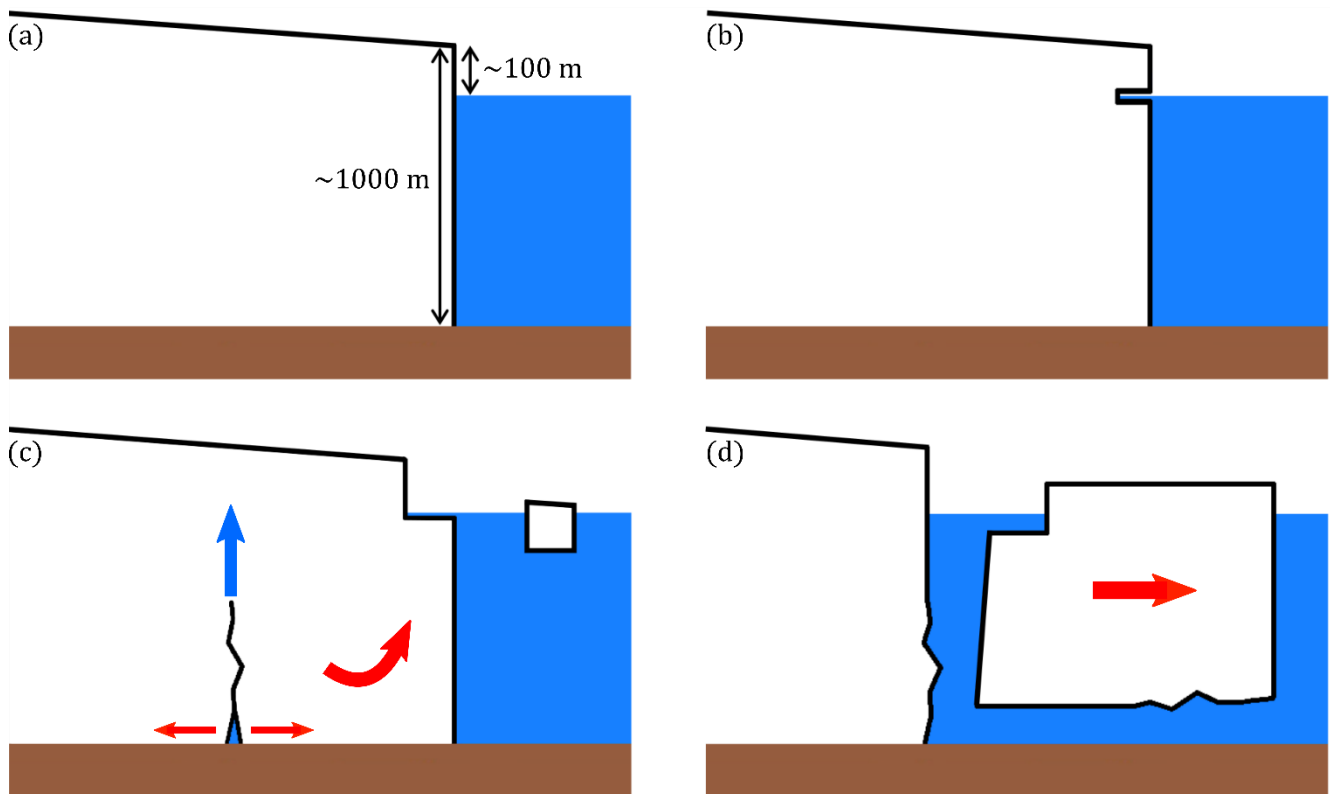
Experiment	Hydraulic connectivity	$l_n$ (m)	$x_1$ (m)	$x_0$ (m)
------------	------------------------	-----------	-----------	-----------

---

F0	Full	0	10000	10000
F100	Full	100	10000	10000
Z0	Zero	0	0	0
Z100	Zero	100	0	0
P0	Partial	0	0	10000
P100	Partial	100	0	10000

**Table 2. Hydraulic connectivity along the ice-bed interface for experiments using the Schoof law. Water pressure is 100% of the full hydrostatic pressure (Eq. 7) downstream of position  $x_1$ . Between  $x_1$  and  $x_0$  water pressure reduces linearly to 0%.**

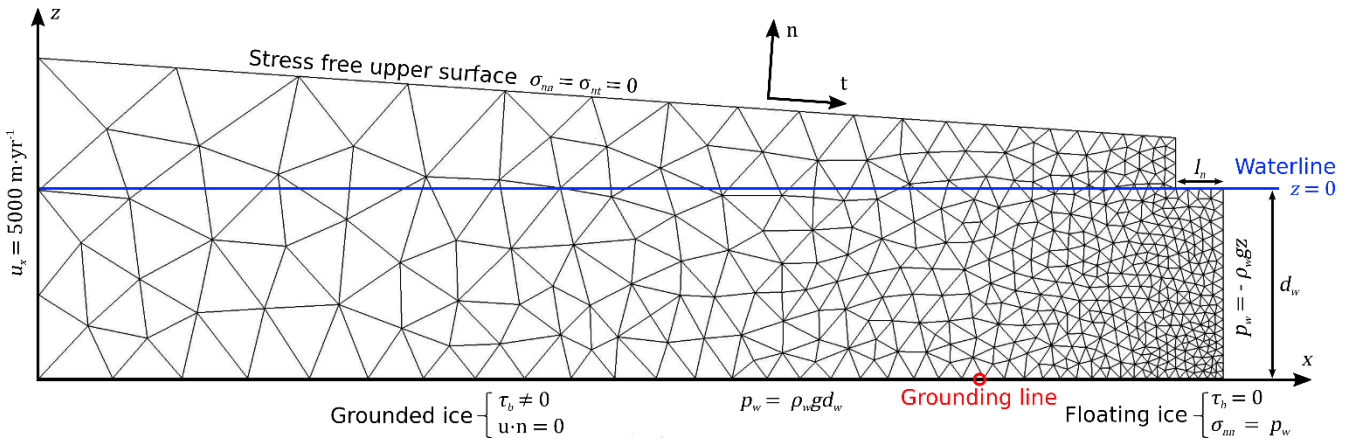
5



10

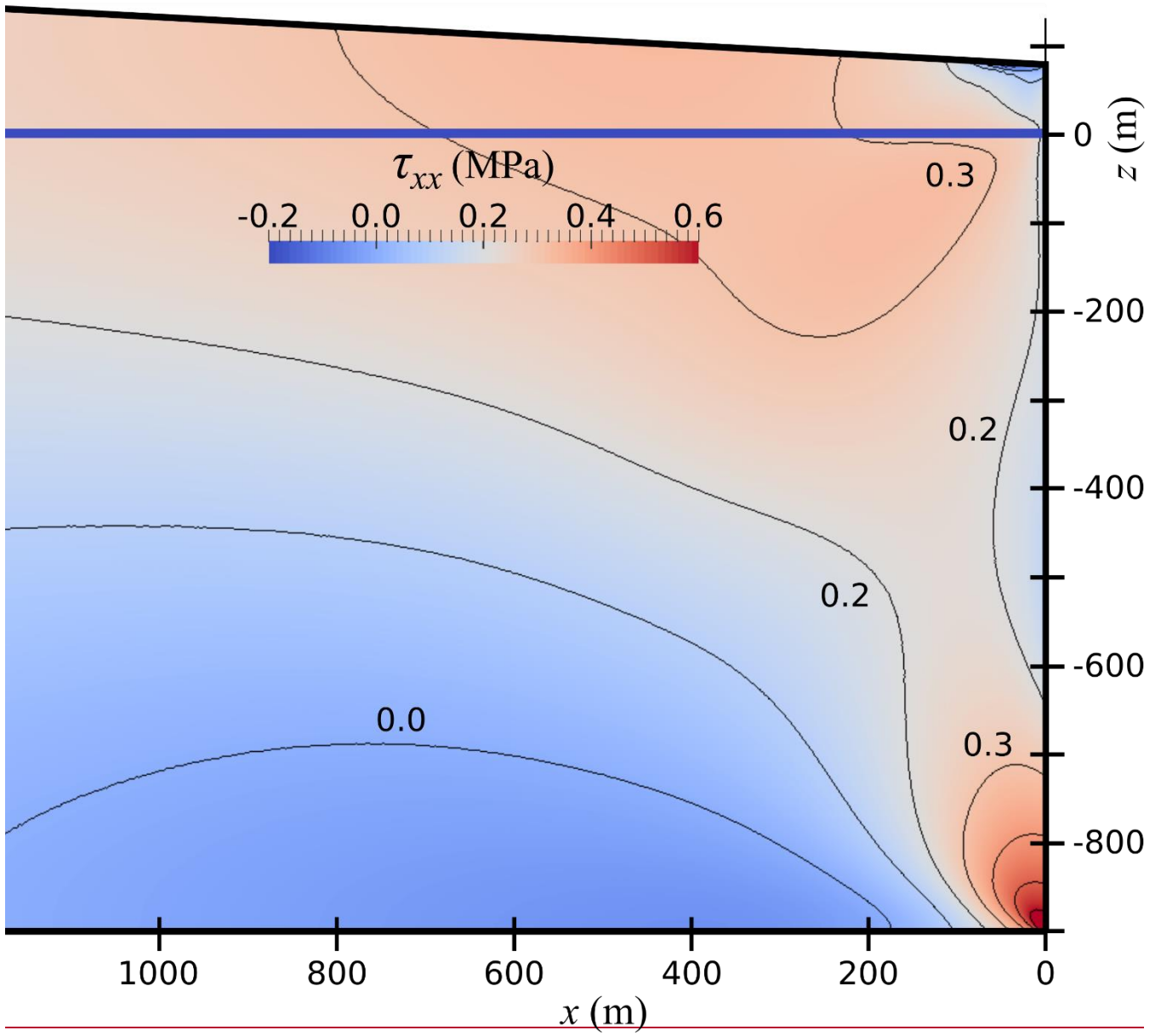
Figure 1. Proposed calving mechanism. (a) Lightly grounded terminus of a tidewater glacier with approximate dimensions of e.g. Jakobshavn Isbræ. (b) A weakness develops in the subaerial section of the front due to (e.g.) undercutting by a wave-cut notch at the waterline. (c) A small subaerial calving event rapidly increases the buoyant load, causing the terminus to tend to lift and rotate. Basal crevasses open and propagate rapidly upwards. (d) Full-depth crevassing results in a large, **rotating-slabbottom-out** calving event. The long-term calving rate is driven by the notch melt rate but is amplified by an unconstrained factor.

5



10

Figure 2. Example mesh and boundary conditions (not to scale). Mesh resolution increases close to the calving front and basal boundaries. Symbols: normal stress  $\sigma_{nn}$ , shear stress  $\sigma_{nt}$ .



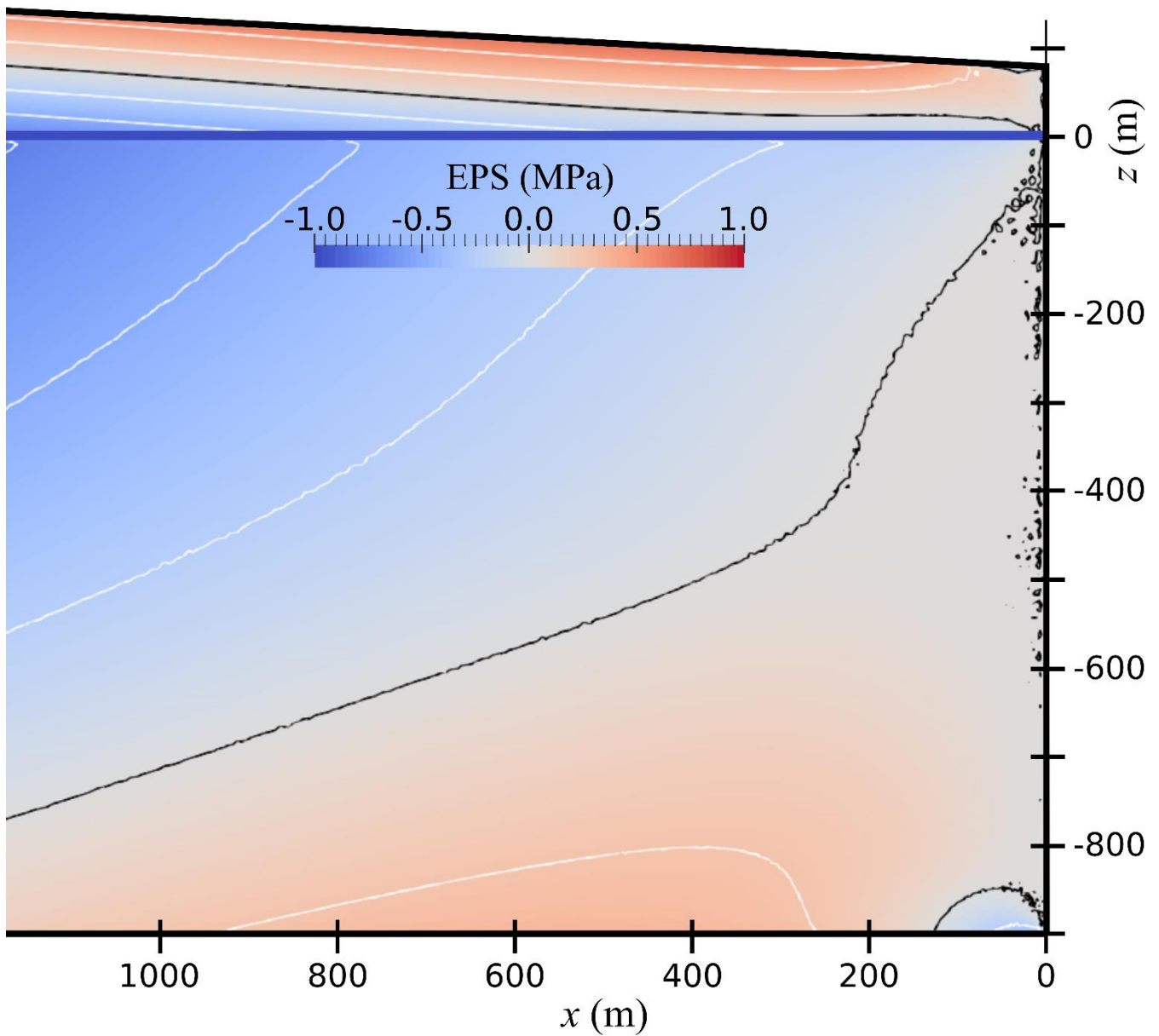
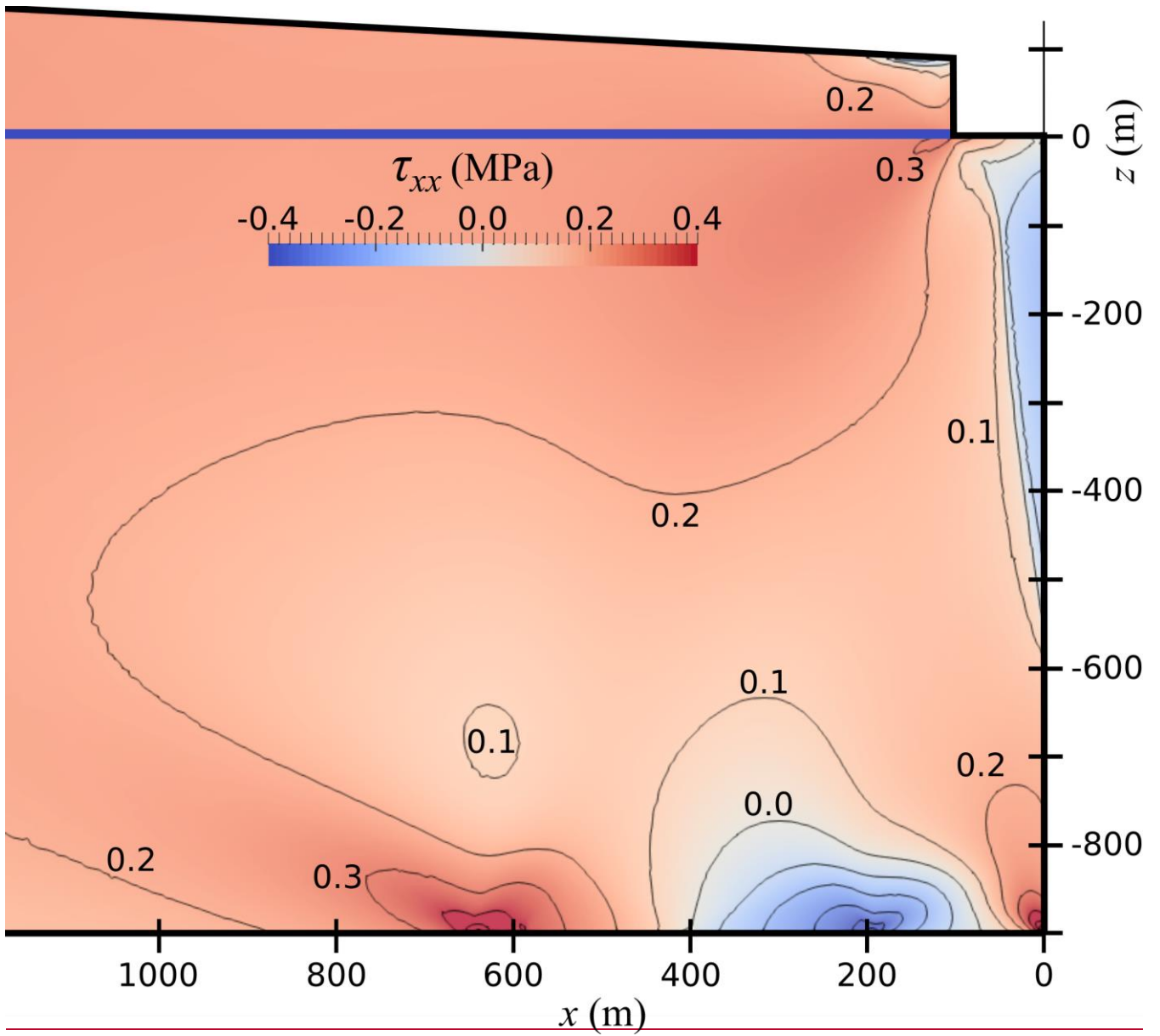


Figure 3. Longitudinal deviatoric Effective principal stress map of the terminus of the glacier before the cutting of a notch, with contours at 0.1 MPa spacing. Note the qualitative similarity to stress maps presented in Hanson and Hooke (2000, 2003).  $d_w = 900$  m,  $h_t = 980$  m,  $\alpha = 3^\circ$  and  $C = 5.623 \times 10^6 \text{ Pa m}^{-1/3} \text{ s}^{1/3}$ . The black contour denotes  $\text{EPS} = 0$  MPa, white contours are spaced at 0.25 MPa intervals.

5



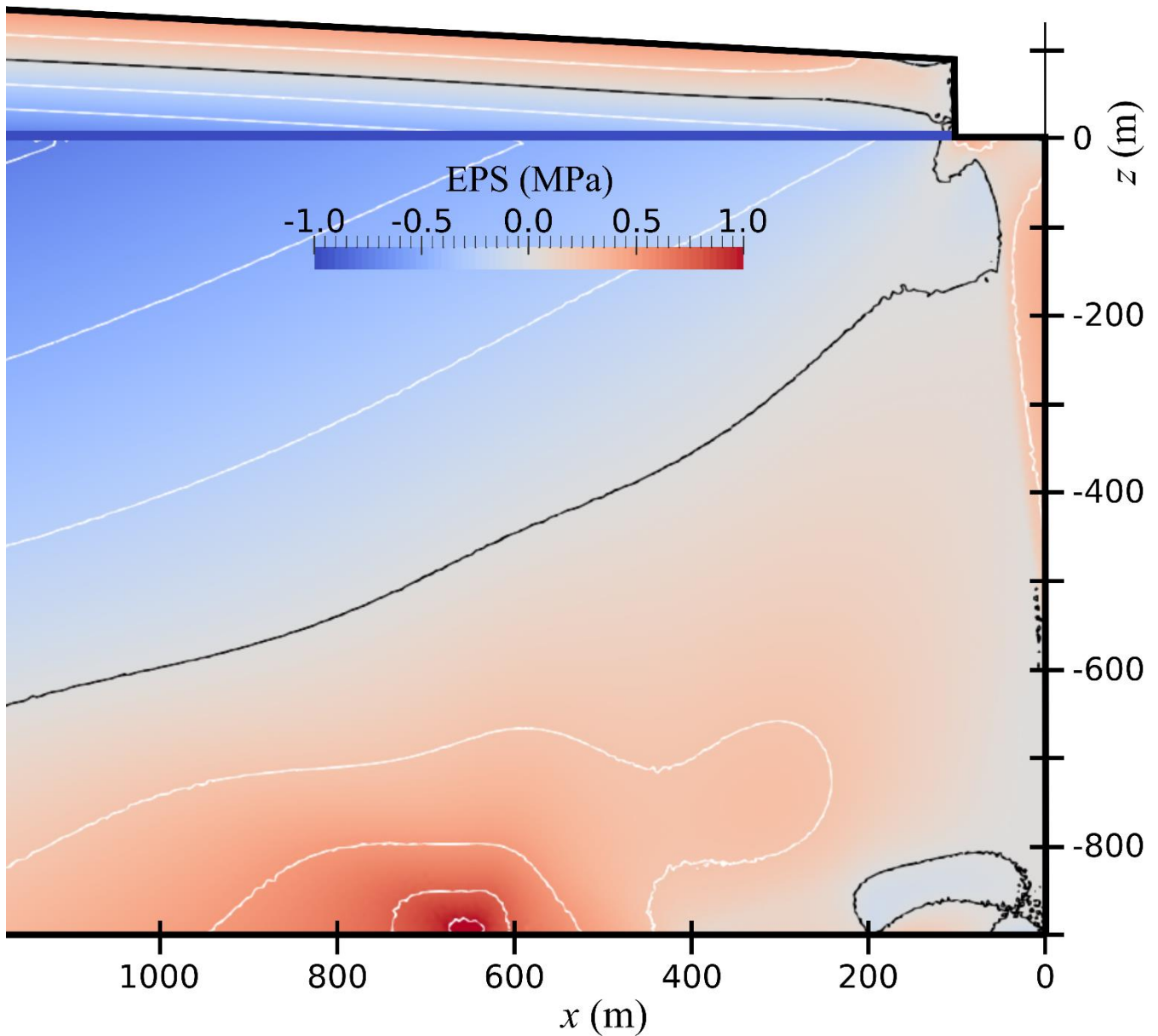
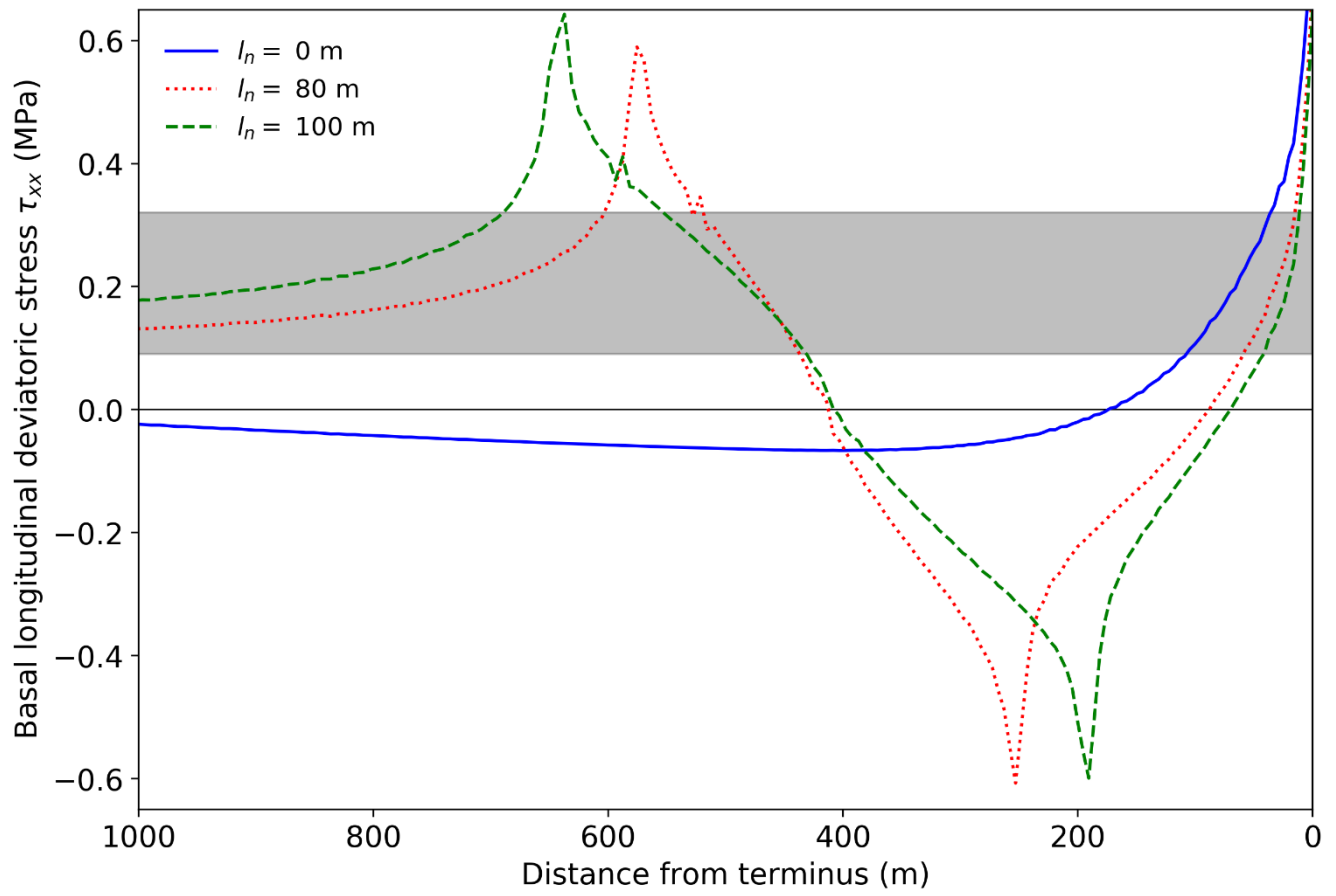


Figure 4. Longitudinal deviatoric Effective principal stress map of the terminus of the glacier with a notch cut to a length  $l_n = 100$  m, with contours at 0.1 MPa spacing.  $d_w = 900$  m,  $h_t = 980$  m,  $\alpha = 3^\circ$  and  $C = 5.623 \times 10^6 \text{ Pa m}^{-1/3} \text{ s}^{1/3}$ . Ungrounding occurred between approximately 1940 m and 6404 m. The black contour denotes  $EPS = 0$  MPa, white contours are spaced at 0.25 MPa intervals.

5



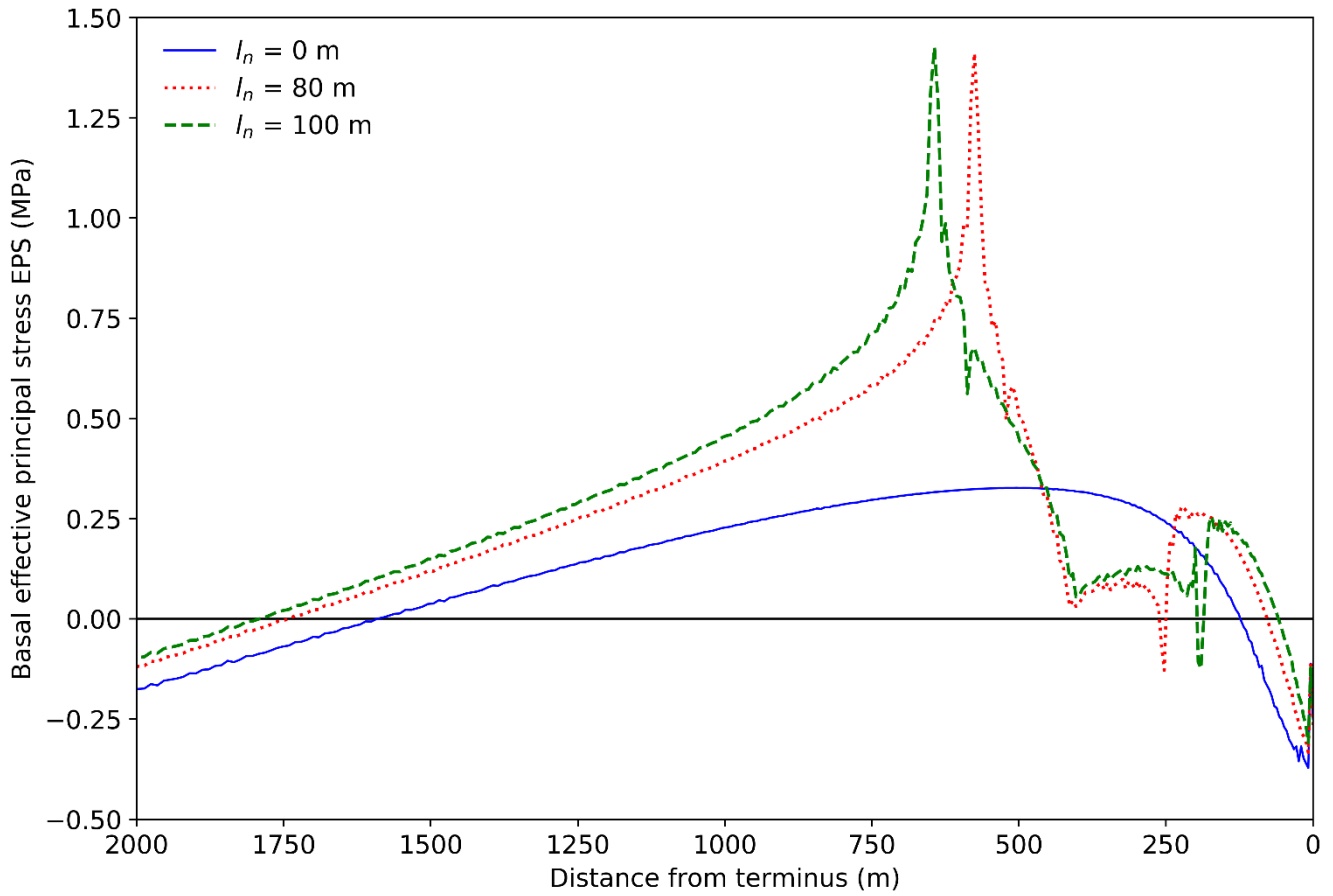
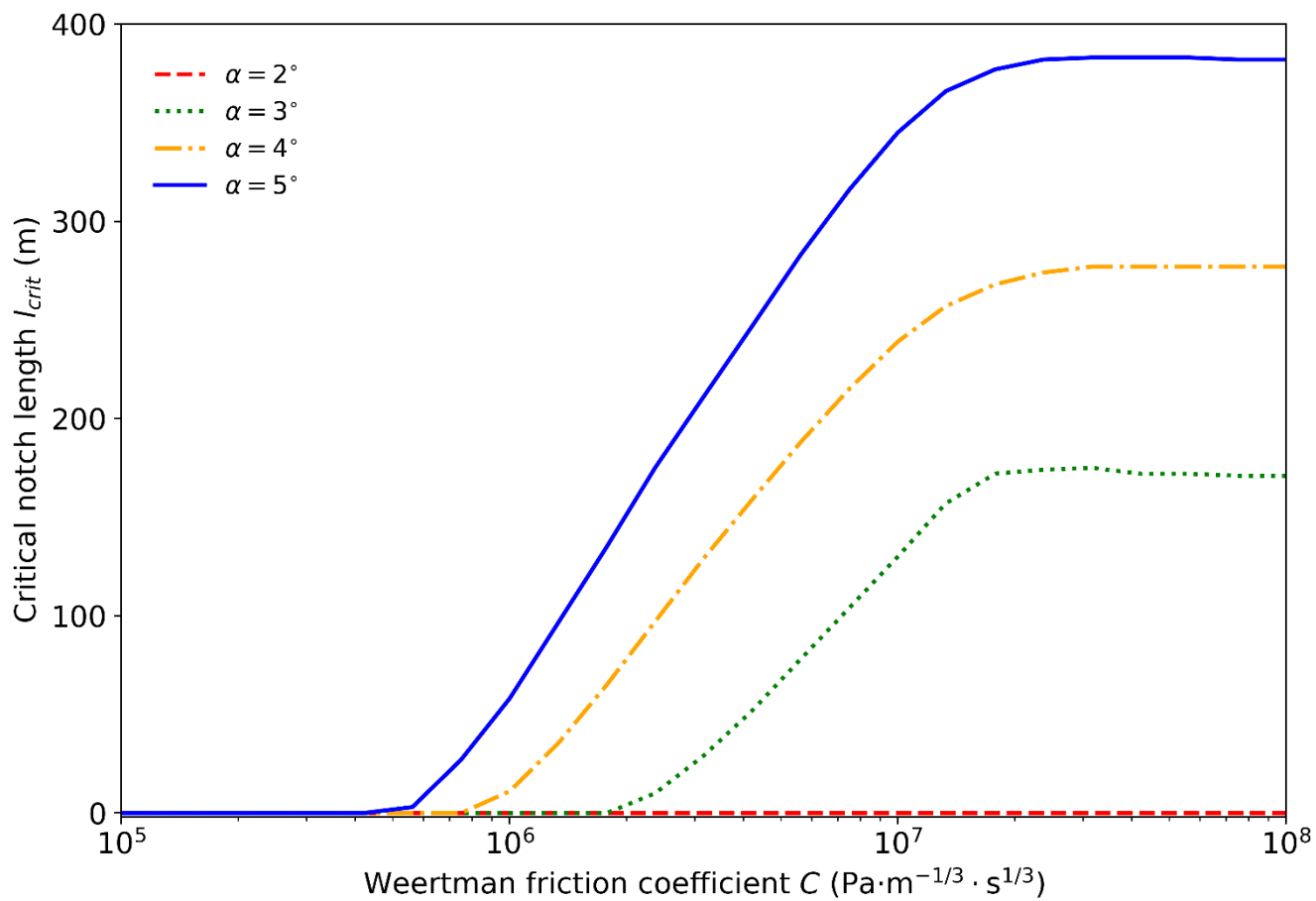


Figure 5. Plots of basal ~~longitudinal deviatoric stress~~ effective principal stress for  $l_n = 0$  m, 80 m and 100 m.  $d_w = 900$  m,  $h_t = 980$  m,  $\alpha = 3^\circ$  and  $C = 5.623 \times 10^6 \text{ Pa m}^{-1/3} \text{ s}^{1/3}$ . ~~The shaded region denotes the tensile strength envelope calculated from Vaughan (1993).~~ The large basal stress concentrations from Fig. 4 correspond to the peak and trough in the  $l_n = 100$  m plot. Ungrounding occurred between approximately 2530 m and 575 m for  $l_n = 80$  m, and between approximately 1940 m and 644-640 m for  $l_n = 100$  m. Note that for this setup, the critical notch length  $l_{\text{crit}} = 79$  m.



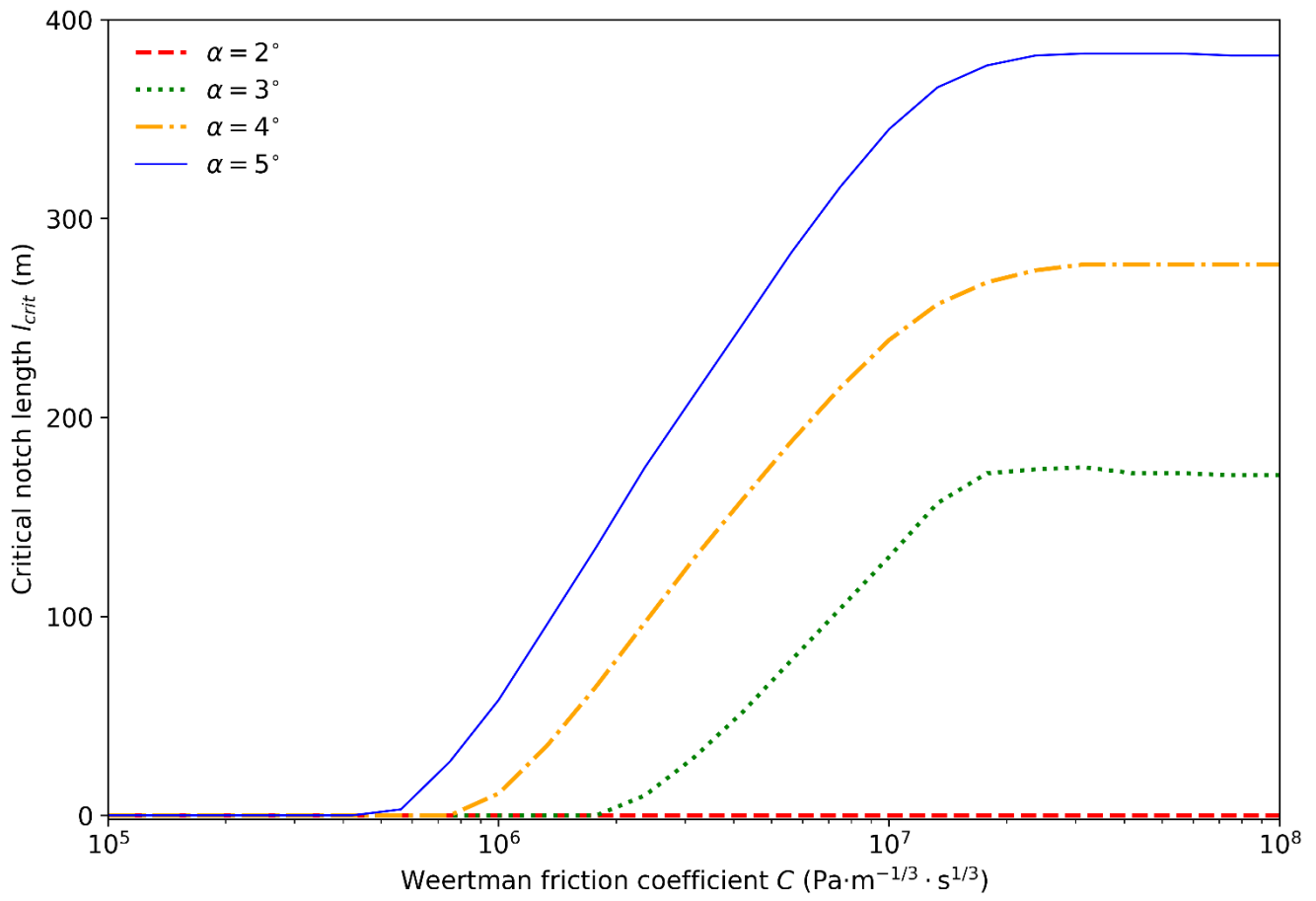
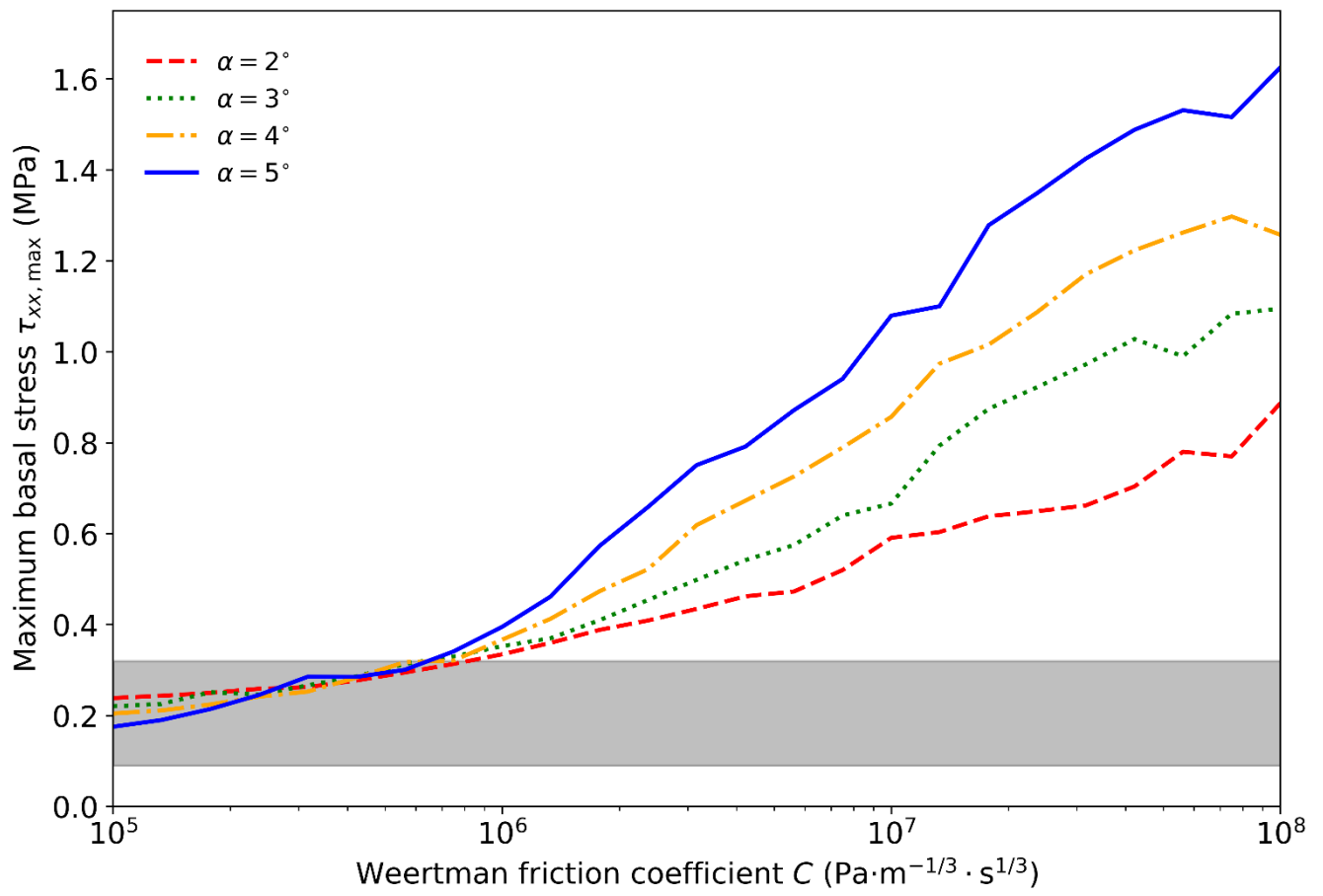


Figure 6. ~~Stress switching~~Critical notch length  $l_{crit}$  plotted for a range of Weertman coefficients  $C$  and surface gradients  $\alpha$ .



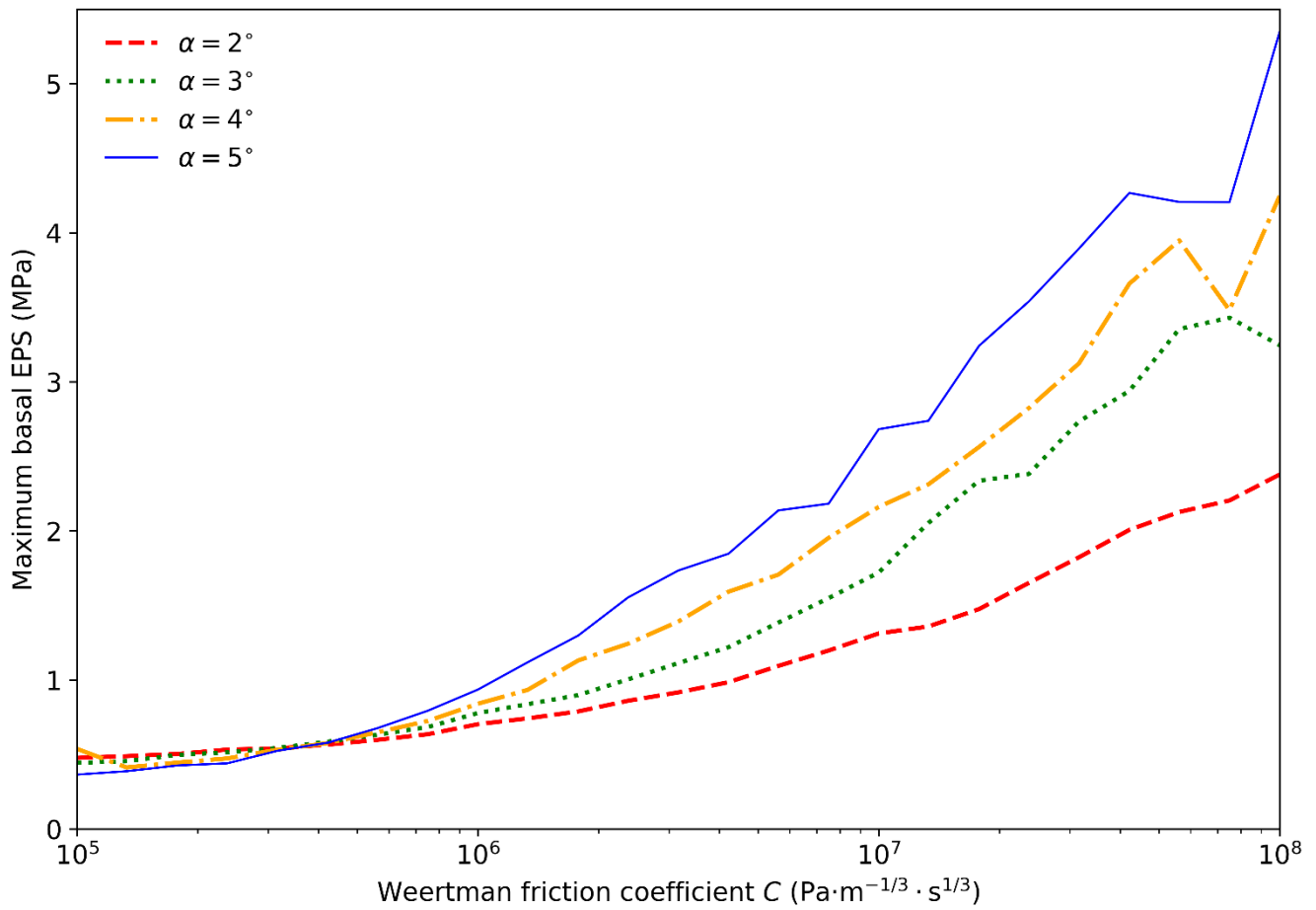
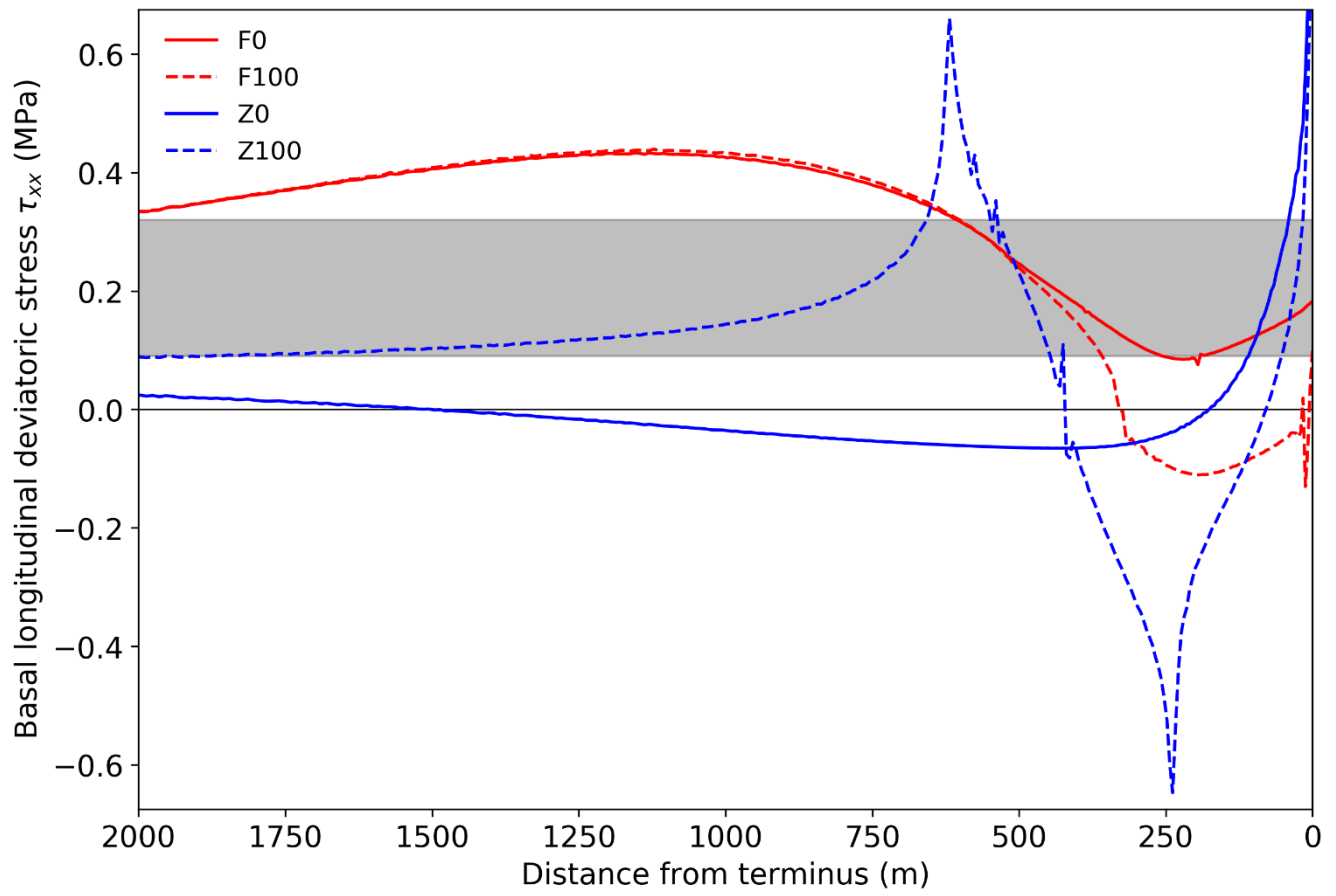


Figure 7. Basal ~~stress~~-EPS maximum plotted with the notch length equal to  $l_{crit} + 25$  m across a range of Weertman coefficients and surface gradients. ~~The shaded region denotes the tensile strength envelope calculated from Vaughan (1993).~~



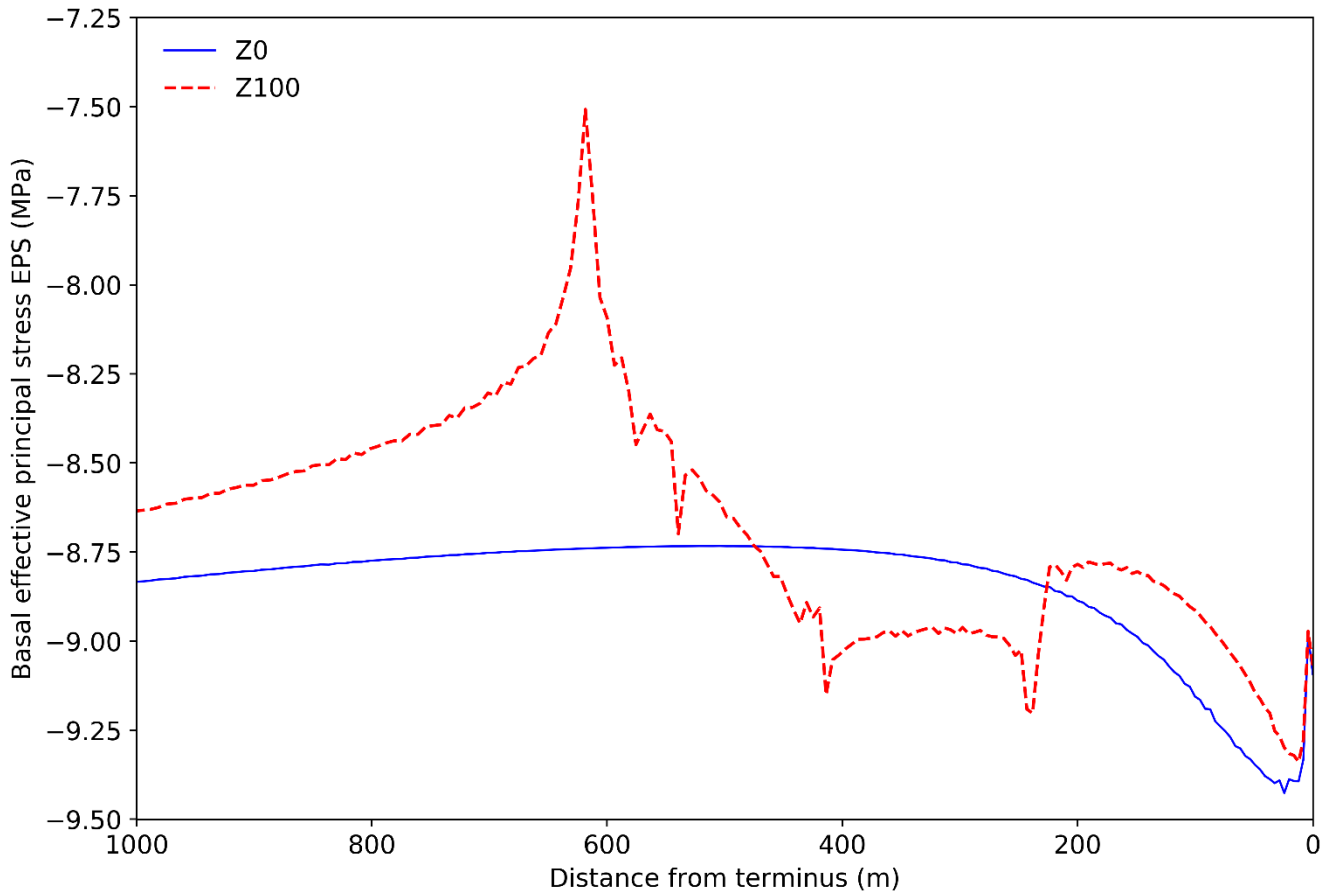
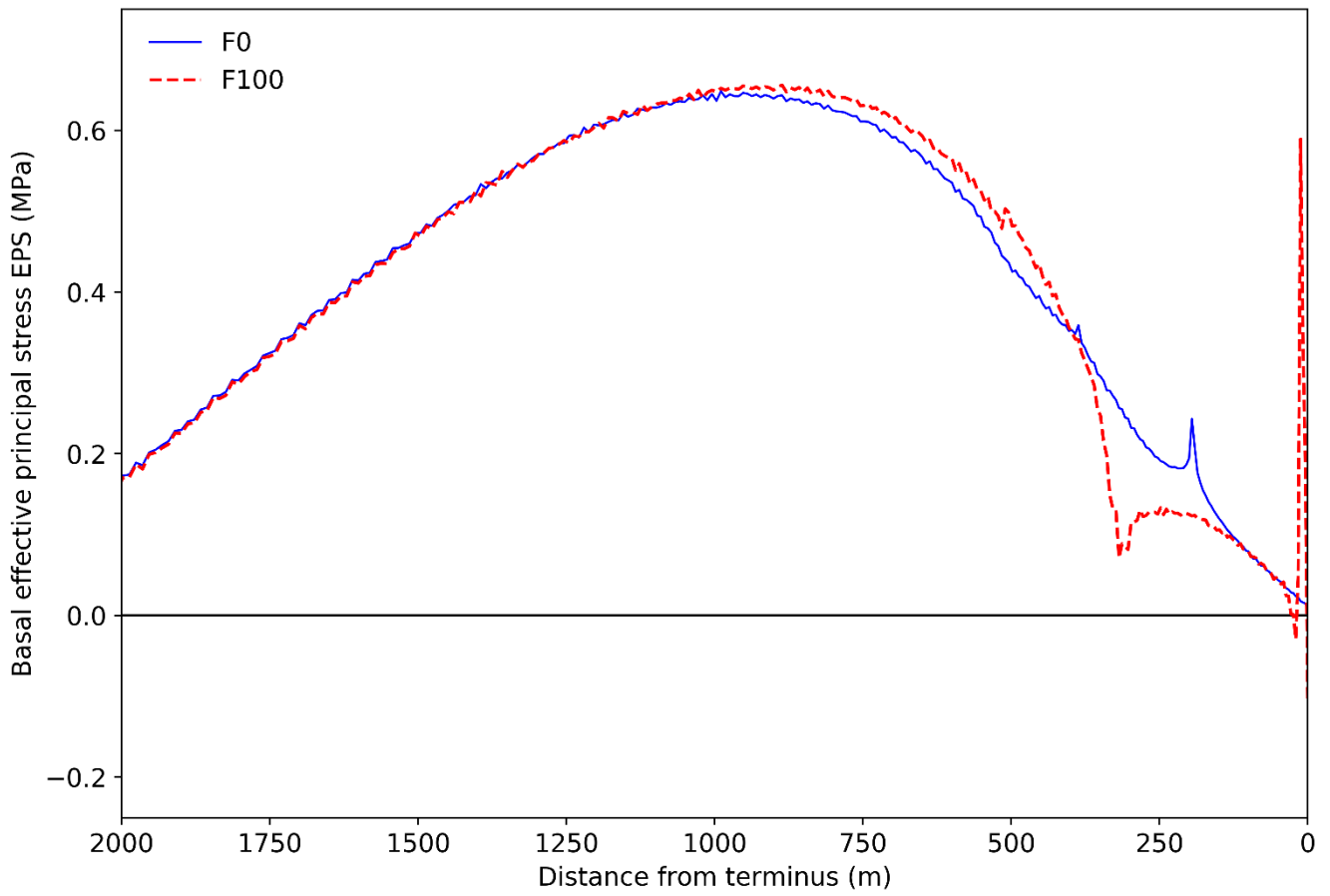
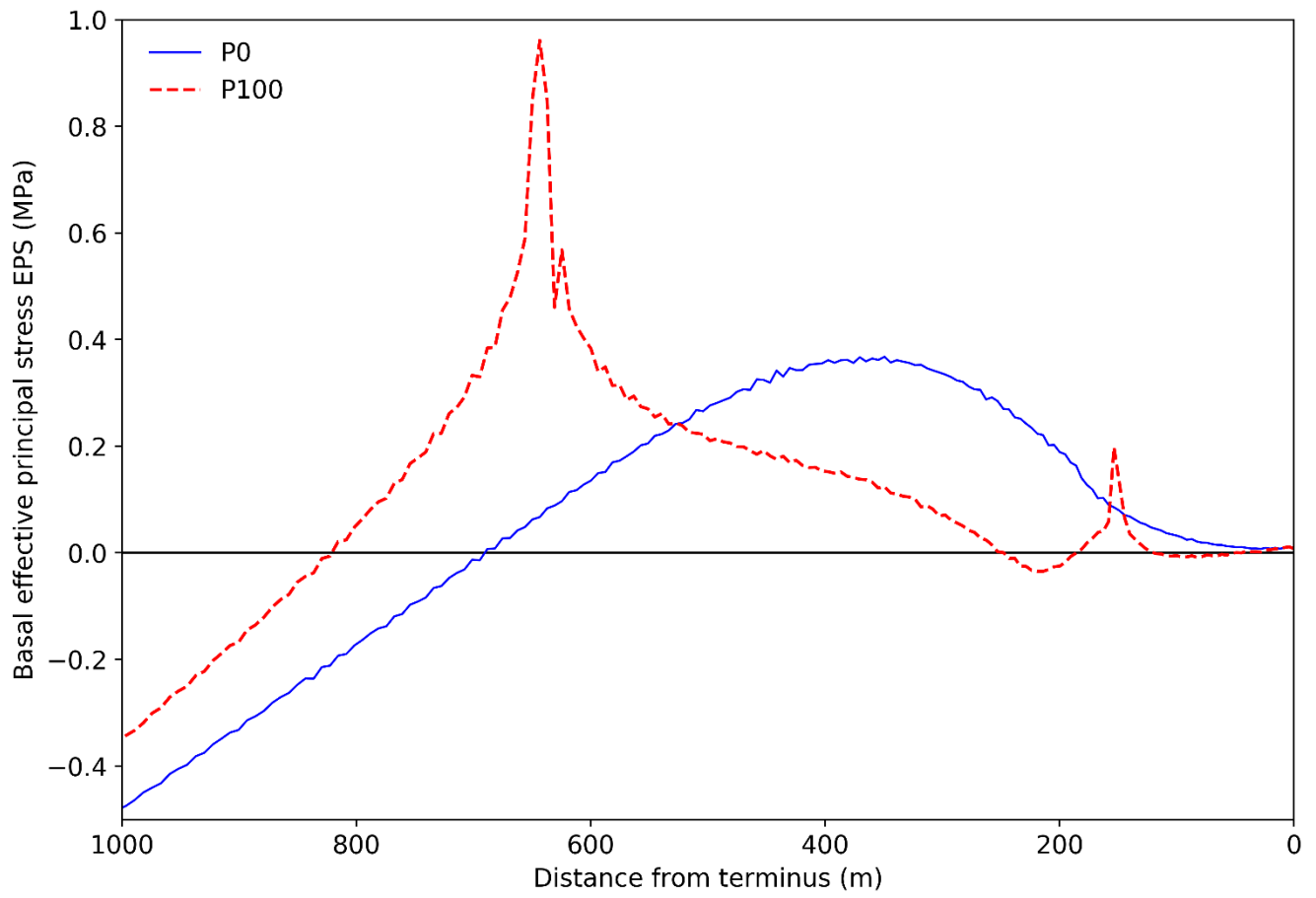


Figure 8. Comparison of basal stresses using the Coulomb sliding law with ~~full (red lines) and zero (blue lines)~~ water pressure ~~inhibited~~ at the ice-bed interface, before (~~solid lines~~Z0) and after (~~dashed lines~~Z100) cutting of a 100 m notch. Ungrounding occurred between approximately 200 m and 3810 m for F0, 16 m and 510 m for F100, and between approximately 243-240 m and 612-610 m for Z100. No ungrounding occurred for Z0.



**Figure 9. Comparison of basal stresses using the Coulomb sliding law with full water pressure at the ice-bed interface, before (F0) and after (F100) cutting of a 100 m notch. Ungrounding occurred between approximately 200 m and 380 m for F0 and between approximately 20 m and 510 m for F100.**



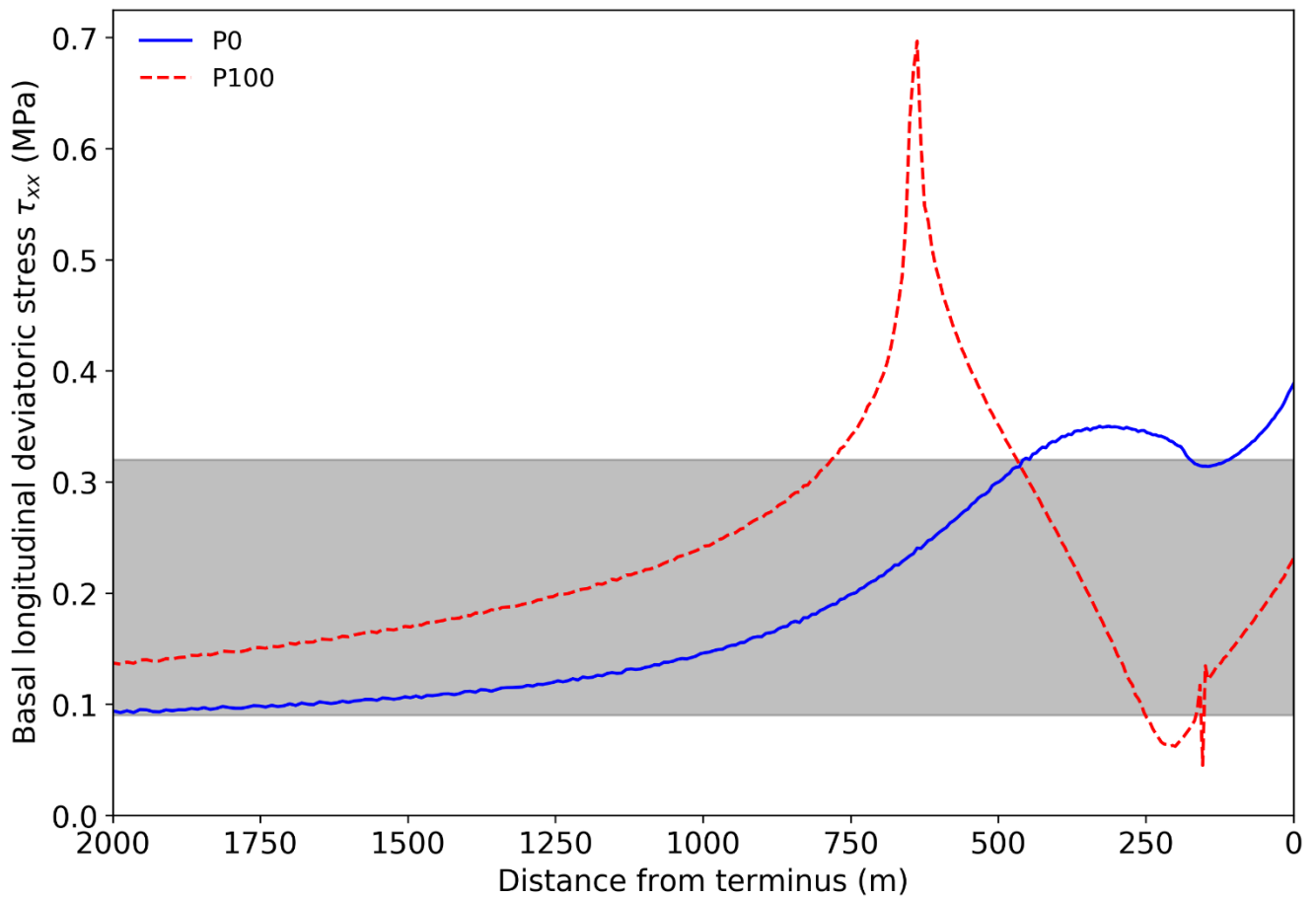


Figure 910. Comparison of basal stresses using the Coulomb sliding law with partial hydraulic connectivity at the ice-bed interface, before (solid blue line P0) and after (red dashed line P100) cutting of a 100m notch. Ungrounding occurred between approximately 158-160 m and 637-640 m for P100 and not at all for P0.